nature geoscience

Supplementary information https://doi.org/10.1038/s41561-026-02039-5

Impacts of power plant emissions on air quality amplified by renewable energy droughts

In the format provided by the authors and unedited

Table of Contents

Dataset S1

Data on installed renewable capacity and national electricity demand collected from existing studies, all targeting the 1.5°C and 2°C warming goals or with high renewable penetration. The dataset includes key variables such as national electricity demand, installed capacity, and electricity generation for various sources, including coal, gas, biomass, hydropower, nuclear, onshore wind, offshore wind, solar, and storage. This dataset offers additional details beyond those presented in Table S1.

Text S1: Electricity system model

We develop an electricity system model for China that simulates hourly power generation from different energy sectors. Unlike optimization models that solve for the optimal generation mix, our model focuses on simulating hourly electricity output based on predefined renewable capacities, leveraging data from prior studies (see Table S1). Designed for easier integration with chemistry-transport models, it operates at the electricity grid level without resolving micro-scale unit operations, enabling efficient large-scale analysis. Fossil fuel power generation is converted to criteria pollutant emissions (Table S2) and spatially allocated using the Dynamic Projection model for Emissions (DPEC) inventory's power sector distribution[1].

S1.1 Definition of the seven Electricity Grids in China

Our electricity model is structured around seven regional grids (Fig. S32) defined by the State Grid Corporation of China (SGCC[2]). For offshore wind integration, we consider only China's exclusive economic zones with water depths <60 m, excluding unsuitable areas (e.g., harbors, shipping lanes, and protected zones) as outlined in Chen et al.[3]. Eligible offshore gridcells are assigned to adjacent onshore electricity grids (North, Northeast, Northwest, East, Central, Southeast, and South). The final spatial distribution of these seven electricity grids is illustrated in Fig. S32. Future projection of the capacity of ultra-high-voltage transmission systems across China in 2050 are also obtained from SGCC.

S1.2 Hourly renewable production

We calculate the wind and solar generation by multiplying the installation capacity (*IC*) with hourly CFs.

$$P_{wind}(t) = IC_{wind} \times CF_{wind}(t)$$

$$P_{solar}(t) = IC_{solar} \times CF_{solar}(t)$$

For nuclear power, we assume operation at rated capacity due to its baseload nature. Hydropower generation is dispatched hourly to compensate for energy deficits, though hourly river runoff data is unavailable. To address this limitation, we apply a simplified model where hydropower partially offsets peak demand. Specifically, hydropower output in our model is scaled proportionally to the residual demand as follows:

$$P_{shortage}(t) = \begin{cases} 0 & if\ Load(t) < P_{subset}(t) \\ P_{subset}(t) - Load(t) & \\ P_{hydro,\,max} & if\ \left(Load(t) - P_{subset}(t)\right) > P_{hydro,\,max} \end{cases}$$

$$P_{subset} = P_{onshore\ wind} + P_{offshore\ wind} + P_{solar} + P_{nuclear} + P_{coal,minimum}$$

Here, $P_{coal,minimum}$ denotes the minimal operating power of coal plants, which is set to be 10% of rated power in the model. We calculate a scaling factor (σ) to distribute the annual total hydropower generation (E_{hydro}) proportionally across periods of energy shortage:

$$\sigma = \frac{E_{hydro}}{\sum_{t=1}^{8760} P_{shortage}(t)}$$

Here, E_{hydro} represents the cumulative annual hydropower potential, provided by literature (see Dataset S1). The hourly hydropower output ($P_{hydro}(t)$) is then determined by scaling the shortage at each time step:

$$P_{hydro}(t) = \sigma P_{shortage}(t)$$

Our battery storage model dynamically tracks the state of charge (SOC) based on the following energy balance equation:

$$SOC(t+1) = SOC(t)(1-\eta) + \theta \times \Delta P(t)$$

Where η is the hourly self-discharge rate (fractional loss per hour; 0.02%), θ is the conversion efficiency (90%) during charging and discharging, $\Delta P(t)$ is the net power flow into/out of the battery at time *t* (positive for charging, negative for discharging). Please note that the hourly charge and discharge rates cannot exceed 25% of the battery maximum capacity. This model operates on an hourly resolution, updating the SOC iteratively at each time step.

S1.3 Operational workflow and validation

The operational strategy of our electricity system model is illustrated in Fig. S2. At each hourly time step *t*, we first calculate the total renewable generation (including wind, solar, nuclear, hydro, and geothermal sources) and compare it with the load demand. When generation exceeds demand, the surplus electricity prioritizes battery charging until either the state of charge reaches 100% or the charging power hits its maximum limit (capped at 25% of total battery capacity per hour). Any remaining excess is then exported to the external grid or curtailed. During periods of generation deficit, the system first draws power from the external grid, then discharges the battery if needed. Only when these resources are exhausted, we activate backup generators (coal, gas, or biomass) to meet the residual demand.

We validate our electricity system model through two approaches. First, the hourly variability of fuel-based power output aligns closely with Energy System Capacity Expansion Model (ESCEM) simulations, which incorporate detailed unit-level characterizations, achieving temporal correlations of 0.91–0.96 (Fig. S3-S5). Second, annual electricity generation in our model matches 24 energy projections with a correlation coefficient of 0.96 and no systematic bias (Fig. S34).

Text S2: Decomposing the effects of REDs into meteorological and emission contributions

Renewable energy droughts (REDs) are often accompanied by unfavorable meteorological conditions that exacerbate air pollution, as well as increased emissions from fossil fuel power plants. Both factors contribute to degraded air quality. To disentangle their respective roles, we apply the following decomposition. In the zero-fossil scenario, where fuel-plant emissions are set to zero, differences in O_3 and $PM_{2.5}$ concentrations between RED and non-RED hours reflect purely meteorological influences(y_{met}). In the with-fossil scenario, which includes dynamically varying fuel-plant emissions, the corresponding concentration differences between RED and non-RED hours reflect the combined effects of both meteorology and emissions (y_{total}). The emission-driven contribution (y_{emis}) is then calculated as $y_{\mathrm{emis}} = y_{\mathrm{total}} - y_{\mathrm{met}}$.

Because both air pollutant concentrations and the occurrence of RED and non-RED hours exhibit seasonal variability, a direct comparison across all hours may introduce biases due to their uneven seasonal distributions. To account for this seasonality, we perform the decomposition separately for each month and then average across months. Specifically, the monthly meteorology-driven and total contributions are first calculated as $y_{met,\,i}$ and $y_{total,\,i}$, where i indexes the month.

The mean contributions are then obtained as

$$y_{met} = \frac{\sum_{i=1}^{n} y_{met,\,i}}{n}$$

$$y_{total} = \frac{\sum_{i=1}^{n} y_{total,\,i}}{n}$$

$$y_{emis} = y_{total} - y_{met}$$

Here, n denotes the number of months included in the analysis.

Text S3: Definition of atmospheric stagnation

Atmospheric stagnation significantly influences the dispersion and accumulation of air pollutants, and its definition varies across regions and studies. In the United States and many previous studies[4,5], an air stagnation day is typically characterized if the 10-m wind speed is below 3.2 m s^{-1}, the 500-hPa mid-tropospheric wind speed is below 13 m s^{-1}, and the precipitation is absent. However, Wang et al.[6] demonstrated that this definition underestimates stagnant weather occurrence in Eastern China. To address this, they proposed a revised definition that retains the 10-m wind speed and precipitation as indicators of horizontal dispersion and wet deposition, respectively, but replaces mid-tropospheric winds with boundary layer height (BLH) to better capture vertical mixing. Stagnant weather is defined by the absence of precipitation and the BLH values below a fitted threshold line, which can be written as:

$$\text{Precipitation} < 1 \text{ mm day}^{-1}$$

$$BLH < a \times e^{-b \times WSP} + c$$

Where WSP refers to wind speeds at 10 meters. The coefficients a, b, and c were empirically derived to optimally capture air pollutant variations across seasons (e.g., spring values: $a=3.57\times10^3$, $b=-3.35$, $c=0.352$)[6]. For each grid cell at hourly resolution, we evaluate whether atmospheric conditions meet stagnation criteria. Regional stagnation intensity is then calculated as the spatial average of grid cells classified as stagnant.

Text S4: Extrapolate hourly O_3 and $PM_{2.5}$ concentrations to all energy scenarios

The nested GEOS-Chem simulation at 50 km resolution over East Asia for a single year requires approximately 15 days using 16 cores of an AMD7763 CPU. Conducting such simulations for all 24 energy scenarios for 6 years, each incorporating multiple meteorological conditions and end-of-pipe emission control policies, would be computationally prohibitive. Thus, to reduce the computation cost, we combine the use of GEOS-Chem simulations and statistical models. More specifically, we run GEOS-Chem simulations for 4 with-fossil energy scenarios (C_1, C_2, C_4, C_{10} in Table S1) and 1 zero-fossil benchmark scenario (C_0). Hourly O_3 and $PM_{2.5}$ concentrations for each gridcell are interpolated across the remaining 19 scenarios.

Taking O_3 as an example, the concentration for the i^{th} gricell and the t^{th} hour under scenario C_j is calculated as:

$$O_3(i,t,C_j) = O_3(i,t,C_0) + k_{O3}(i,t)\, G(i,t,C_j)$$

Where $O_3(i,t,C_j)$ denotes the O_3 concentrations under scenario C_j, and $O_3(i,t,C_0)$ is the corresponding concentration in the zero-fossil scenario C_0. $G(i,t,C_j)$ refers to the NO emissions from fossil electricity generation. The coefficient $k_{O3}(i,t)$ represents the sensitivity of O_3 concentrations to NO emissions of fossil fuel electricity generation at the i^{th} gricell and the t^{th} hour. The values are derived from GEOS-Chem simulations for scenarios C_0, C_1, C_2, C_4 and C_{10} for each grid cell and hour. The coefficient of determination (R^2) of these regressions ranges from 0.95 to 0.99, indicating high predictive accuracy. This hourly-scale regression captures the non-linear responses of O_3 to anthropogenic emissions under varying meteorological and emission conditions more accurately than regressions performed at monthly or annual scales. This approach significantly enhances the representation of emission impacts while reducing computational costs.

An analogous analysis is also applied to $PM_{2.5}$ concentrations, with explicit treatment of its major chemical components expressed as

$$PM_{2.5}(i,t,C_j) = PM_{2.5}(i,t,C_0) + k_{PM2.5}(i,t)\,G(i,t,C_j)$$

To account for $PM_{2.5}$ chemical complexity, this regression is performed separately for sulfate, nitrate, and fine dust, using SO_2, NO and $PM_{2.5}$ emissions from fossil fuel plants as predictors, respectively. Changes in ammonium are diagnosed from associated changes in sulfate and nitrate according to stoichiometric constraints $\Delta Ammonium = 2 \times \frac{18}{96}\Delta sulfate + \frac{18}{63}\Delta nitrate$, where 18, 96 and 63 refers to the molar masses for ammonium, sulfate and nitrate.

Text S5: Comparison of our health cost from fuel-based plants with Chen et al.[7]

A comparison with Chen et al.[7] reveals some differences in estimated health costs, primarily driven by methodological assumptions. Chen et al.[7] consider health impacts only from $PM_{2.5}$, excluding ozone (O_3), and focus on present-day conditions, reporting health costs of 12.3 cents kWh^{-1} (USD) for coal power plants in 2017 and 0.77 cents kWh^{-1} (USD) for gas plants in 2024. In contrast, our analysis targets future conditions in the 2050s. When we adopt the same population age structure as in current years, our estimated health costs are 0.65 cents kWh^{-1} (USD) for coal and 0.27 cents kWh^{-1}(USD) for gas— both lower than those reported by Chen et al. [7]

To enable a direct, like-for-like comparison, we further recalculate health costs using the same emission factors for coal and gas plants, and the same value of statistical life (VSL) as in Chen et al[7]. Under these harmonized assumptions, our estimates are 13.2 cents kWh^{-1} (USD) for coal and 0.95 cents kWh^{-1} (USD) for gas, in close agreement with Chen et al[7]. This indicates that the discrepancies primarily arise from differences in emission factors and VSL assumptions. In the following sections, we justify our choice of emission factors and VSL assumptions as more appropriate for assessing health impacts in China under future energy pathways.

S5.1 Emission factors

Table S9 compares the emission factors adopted in the two studies. For coal-fired power plants, Chen et al. (2024) use emission factors that are approximately four times higher than those in our study. This difference reflects the distinct study periods: Chen et al. [7] quantify health impacts from the existing coal plants in 2017, whereas our analysis targets future power plants in the 2050s, assuming deployment of best-available emission control technologies. For gas-fired power plants, Chen et al. [7] assume exceptionally stringent controls, with a NO_x emission factor of 0.107 g kWh^{-1}—about half of the lowest emission levels observed for current gas plants globally (e.g., 0.23 g kWh^{-1} in the United States[8]). In contrast, our emission factors are derived from the DPEC inventory for the 2050s and are comparable to present-day global best-practice levels (~0.23 g kWh^{-1})[8], and therefore higher than those assumed by Chen et al. [7].

S5.2 Value of a statistical life (VSL)

The discrepancy in estimated health costs between our study and Chen et al. [7] also arises from a large difference in the valuation of the VSL values. Chen et al. [7] derived China's VSL by transferring a U.S. baseline value ($VSL_{base,US}$ = USD 7.4 million per person in 2006 [9]) using a GDP-scaling approach:

$$VSL_{CN} = VSL_{base,US} \times (pcGDP_{CN}/pcGDP_{US})^{0.5}$$

Using $pcGDP_{CN}$ 8,989 USD (2017) and $pcGDP_{US}$ 46,000 USD (2006), the VSL_{CN} is estimated at $3.2 million per person in China.

In contrast, our analysis uses a VSL grounded in recent China-specific research from Yin et al. [10]. It uses the age-adjusted values of life (VSL) and the statistical life-years (VSLY)[10], which account for the influence from remaining life expectancy, life quality, and wealth weights. These estimates yield an average VSL of approximately 0.7 million (USD) in China, consistent with an independent six-city survey (n = 3,936) that reported a VSL of 0.69 million (USD) in 2019[11]. We further refine this estimate by accounting for the differential impact of air pollution across age groups. Since air pollution disproportionately affects the elderly, and both VSL and VSLY values decrease with age. By including the age impacts of air pollution in the calculation, the estimated health cost due to every mortality needs to be scaled by a factor of 0.65, which is approximated 0.69 ×0.65=$0.45 million USD. Consequently, the VSL used by Chen et al. [7]（$3.2 million）is roughly ~7 times higher than our age-adjusted, China-specific estimate ($0.45 million).

S5.3 Step-to-step reproduction of health cost of Chen et al.

Table S10 compares the estimated health costs from fossil fuel power plant emissions in this study with those reported by Chen et al. Through Experiments 1–3, we progressively harmonize key assumptions—emission factors, population age structure, and VSL valuation—with those of Chen et al. [7] When all parameters are aligned (Experiment 3), we closely reproduce their reported health costs, confirming that the differences between the two studies primarily stem from emission factors and VSL assumptions. Because Chen et al. [7] focus on present-day emissions, whereas our analysis targets future power systems, the dominant source of divergence ultimately lies in the choice of VSL. As shown in Text S5.2, the VSL values adopted in our study are consistent with an independent six-city contingent valuation survey and explicitly account for age-specific vulnerability to air pollution. These features suggest that our approach provides a more appropriate and policy-relevant estimate of health costs for China in a future-oriented context.

Text S6. Optimization of renewable energy expansion

Fig. 5 in the main text outlines our approach to determining the economically optimal level of renewable energy expansion. We focus on wind and solar power, which represent the most scalable renewable resources in China, whereas hydropower and nuclear expansion is constrained by resource availability and policy considerations[3]. For each energy scenario, we apply an incremental scaling factor (SF_i, i=1-21) ranging from 0% to 100% in 5% intervals to wind and solar capacity.

Step 1. For each SFi, we run the electricity system model to compute hourly electricity generation from all renewable and fossil fuel sources. As wind and solar capacity increases, renewable generation rises, and fossil fuel generation correspondingly declines. Using Eq. 8, we calculate the marginal LCOE of additional wind and solar capacity ($LCOE_i$) at each expansion level.

Step 2. The reduction in fossil fuel generation under each SF_i is translated into avoided emissions of NO_x, SO_2, and primary $PM_{2.5}$, which are further converted into changes in O_3 and $PM_{2.5}$ concentrations and monetized as health benefits. In parallel, we quantify avoided fuel costs and CO_2 emissions costs. In this step, we assume that the cost per kilowatt-hour (kWh) of electricity generated from fossil fuel plants remains constant.

Step 3. The optimal expansion level is identified by comparing marginal LCOE — which rises as SF_i increases due to greater curtailment rates— with the total avoided cost per kWh of fossil fuel generation, which is held constant. By evaluating these metrics across all SF_i values, we solve for the point where the marginal LCOE equals the total avoided cost. This procedure is applied consistently across all scenarios, with the resulting optimal fossil fuel penetration rates summarized in Fig. 5d.

Our framework to evaluate the air impacts of fossil fuel plant emissions

(a) Integration of the electricity model with GEOS-Chem

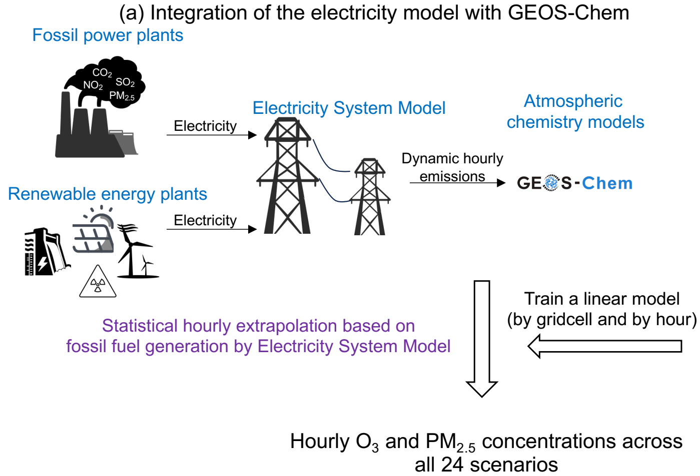

(b) Air quality impacts simulated by GEOS-Chem

Energy scenario	Non-power emissions	Meteorology	Fossil fuel plant generation (PWh)
Case 0 (zero-fossil benchmark)	1.5℃ goals	MERRA2	0.00
	2℃ goals	MERRA2	
	1.5℃ goals	GISS ModelE2	
Case 2 (representative with-fossil scenario)	1.5℃ goals	MERRA2	2.10
	2℃ goals	MERRA2	
	1.5℃ goals	GISS ModelE2	
Case 1	1.5℃ goals	MERRA2	4.76
Case 4	1.5℃ goals	MERRA2	6.61
Case 19	1.5℃ goals	MERRA2	0.90

Fig. S1. Our framework to evaluate the air impacts of fossil fuel plant emissions in China. The electricity generation is modelled on an hourly basis. The chemistry transport model, GEOS-Chem, includes a detailed description of ozone and aerosol chemistry at a spatial resolution of 50km. The emission factors used to calculate emissions from power plants are shown in Fig. S6 and Table S2. The right panel indicates the energy scenarios for which air quality impacts are simulated explicitly with GEOS-Chem; impacts for the remaining scenarios are estimated using regression models. Energy scenarios are defined in Table S1, where C0 denotes the zero-fossil benchmark and C2 represents the reference with-fossil scenario. Scenarios C1, C2, C4, and C19 are selected for GEOS-Chem simulations because they span a wide range of fossil fuel electricity shares (6–36%), capturing the diversity of future energy system projections considered in this study.

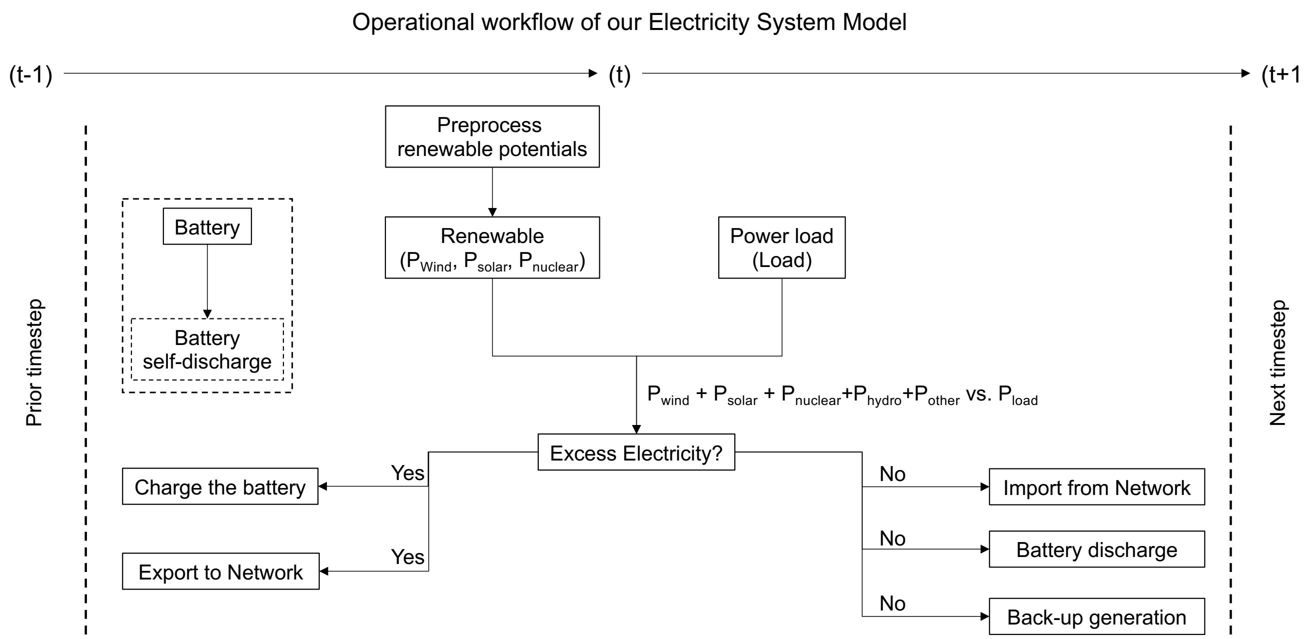

Fig. S2. The operational workflow of our electricity system model. Unlike optimization models that determine the optimal generation mix, this electricity model simulates hourly electricity output based on predefined renewable capacities (Table S1). See Text S1 for more details.

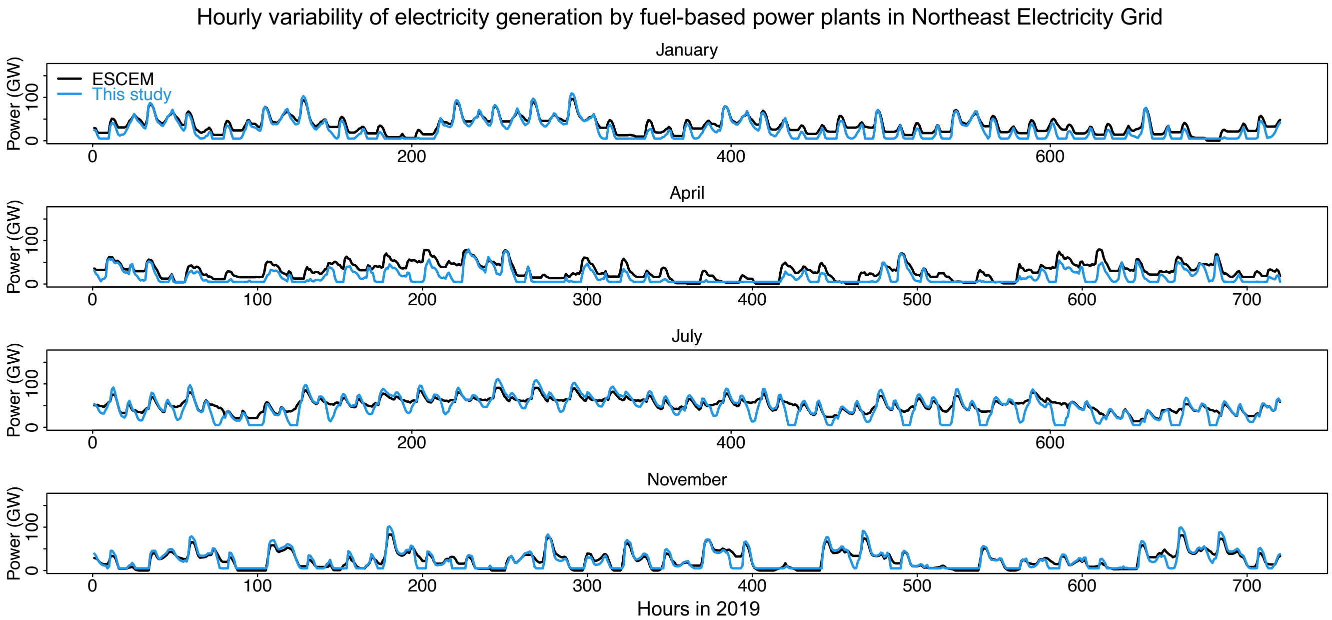

Fig. S3. **Hourly variability of electricity generation by fossil fuel power plants from our electricity model and the Energy System Capacity Expansion Model (ESCEM[12]) in Northeast Electricity Grid**. The ESCEM includes detailed facility- to national-scale processes. Results are shown for 4 representative months in the year 2019. See Fig. S32 for the location of this electricity grid. The correlation coefficient between two timeseries is 0.91.

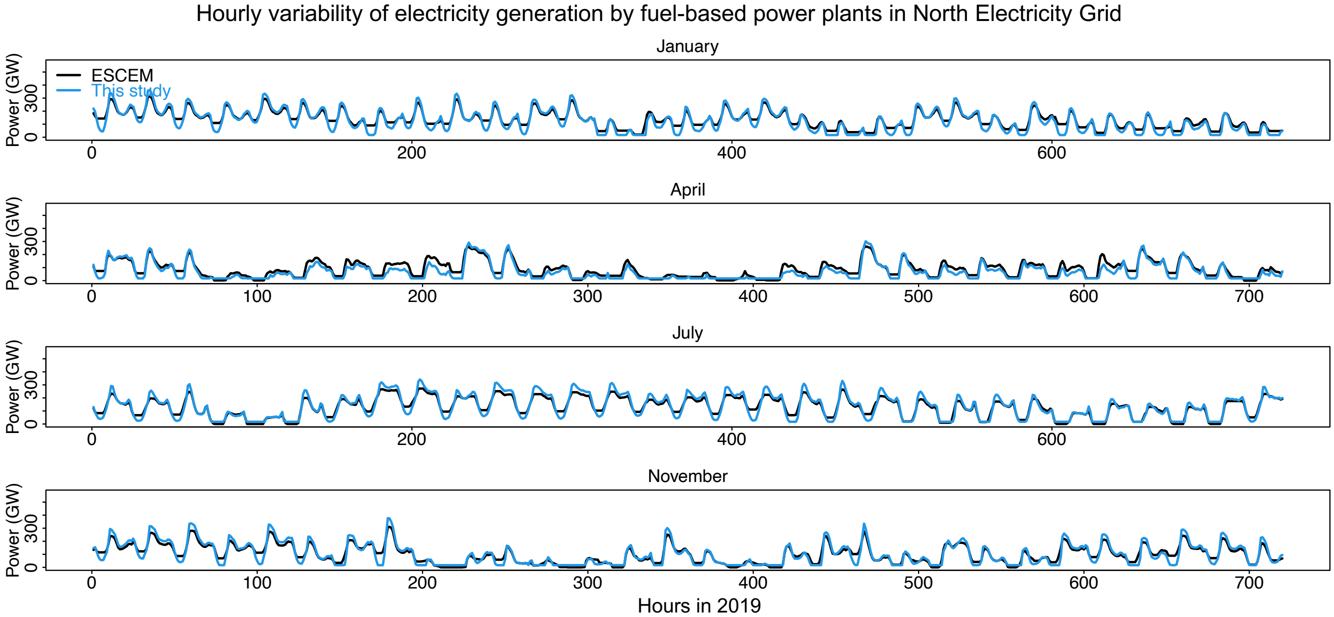

Fig. S4. **Hourly variability of electricity generation by fossil fuel power plants from our electricity model and the Energy System Capacity Expansion Model (ESCEM[12]) in the North Electricity Grid**. The ESCEM includes detailed facility- to national-scale processes. Results are shown for 4 representative months in the year 2019. See Fig. S32 for the location of this electricity grid. The correlation coefficient between two timeseries is 0.96.

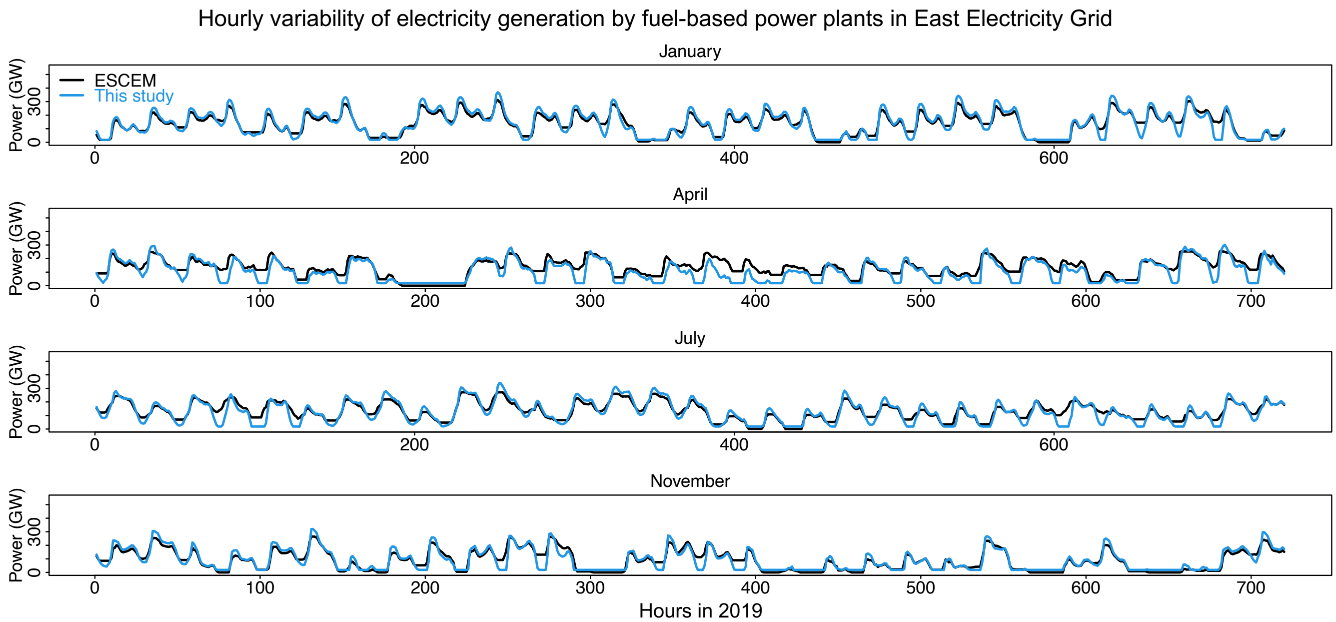

Fig. S5. **Hourly variability of electricity generation by fossil fuel power plants from our electricity model and the Energy System Capacity Expansion Model (ESCEM[12]) in East Electricity Grid**. The ESCEM includes detailed facility- to national-scale processes. Results are shown for 4 representative months in the year 2019. See Fig. S32 for the location of this electricity grid. The correlation coefficient between two timeseries is 0.93.

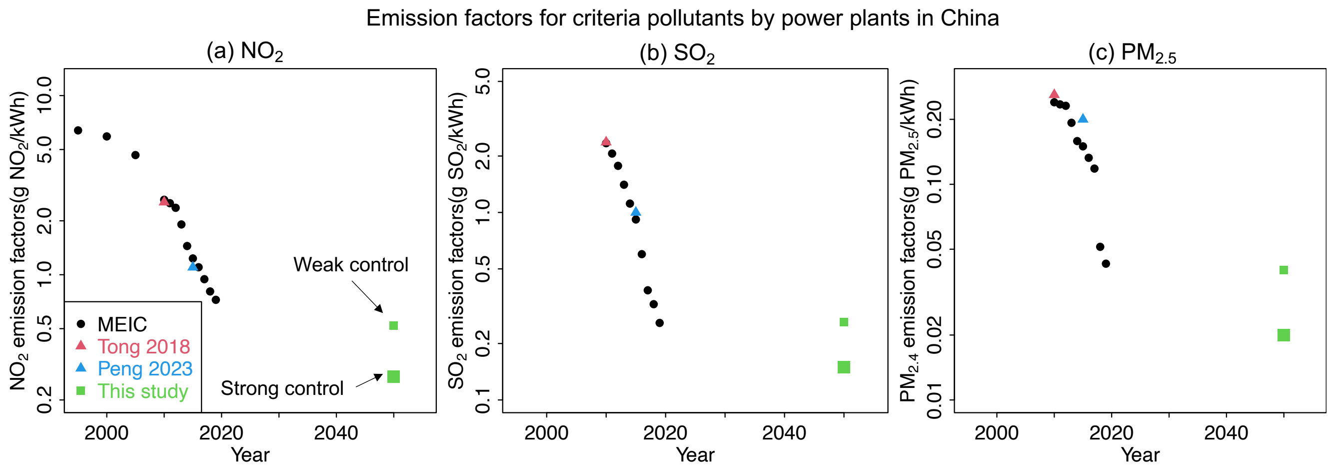

Fig. S6. Emission factors for criteria pollutants (NO_2, SO_2 and $PM_{2.5}$) emitted by coal power plants from 2000 to 2050 in China. The data from 2000 to 2020 is from the MEIC inventory[13], compared with studies Tong et al.[8] and Peng et al[14]. For the emission factors in 2050, we present the values with strong and weak emission control policies obtained from the Dynamic Projection model for Emissions in China (DPEC) inventory [1,8,15]. The detailed values of emission factors for both coal and gas plants can be found in Table S2.

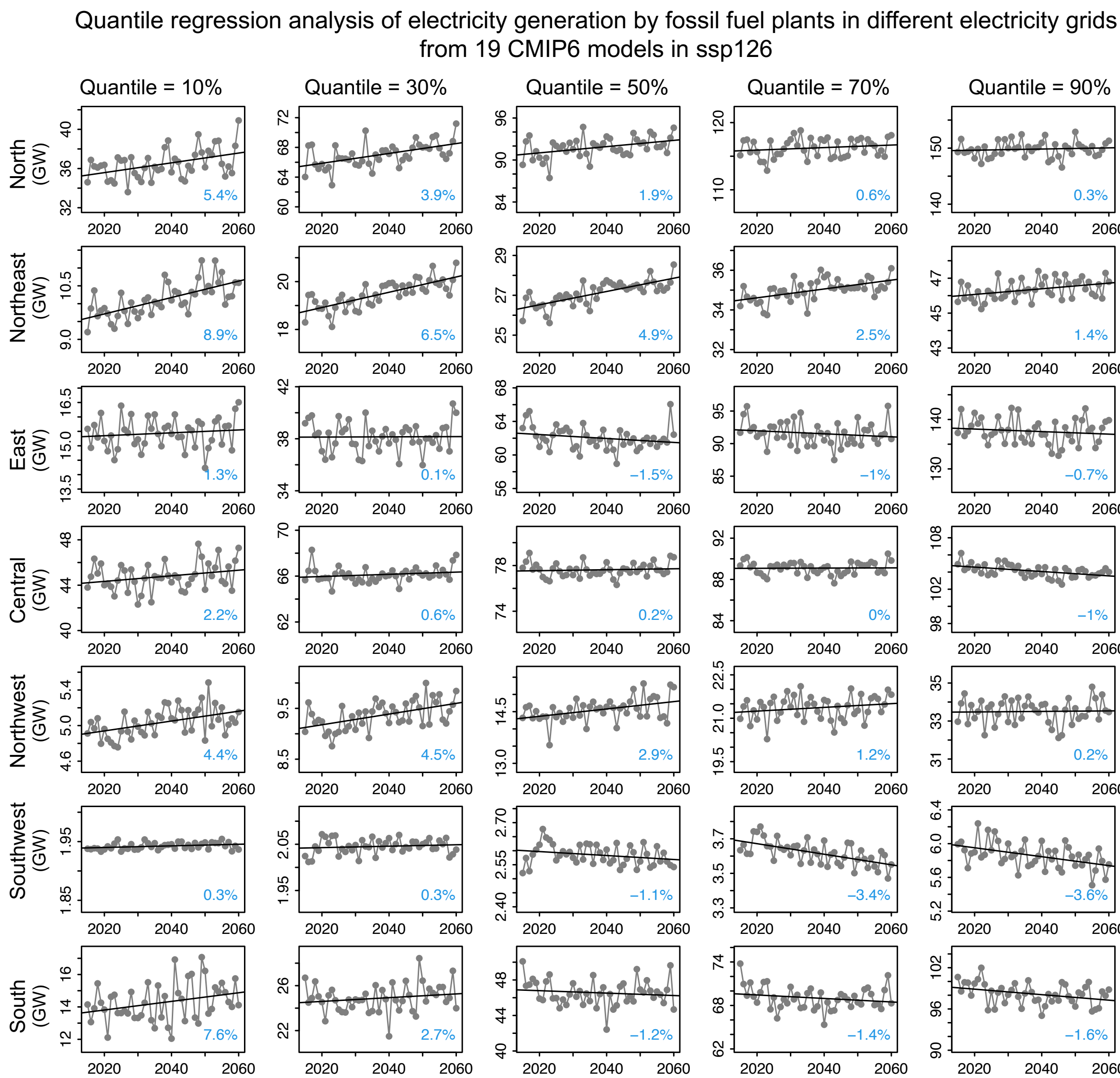

Fig. S7. **Quantile regression analysis of electricity generation from fossil fuel plants in different electricity grids from 2015 to 2060, based on 19 CMIP6 models (see Table S3) under the SSP126 scenario**. Results are shown for quantiles from 10th, 30th, 50th, 70th, and 90th percentiles. In this analysis, hourly wind and solar radiation data from CMIP6 models are input into the electricity grid model, which outputs the electricity generation from power plants. Here, we use the representative with-fossil scenario from Chen et al.[3] (C2 in Table S1), which assumes an 84% renewable penetration rate. The percent change (blue texts) denotes the relative changes from 2015 to 2060.

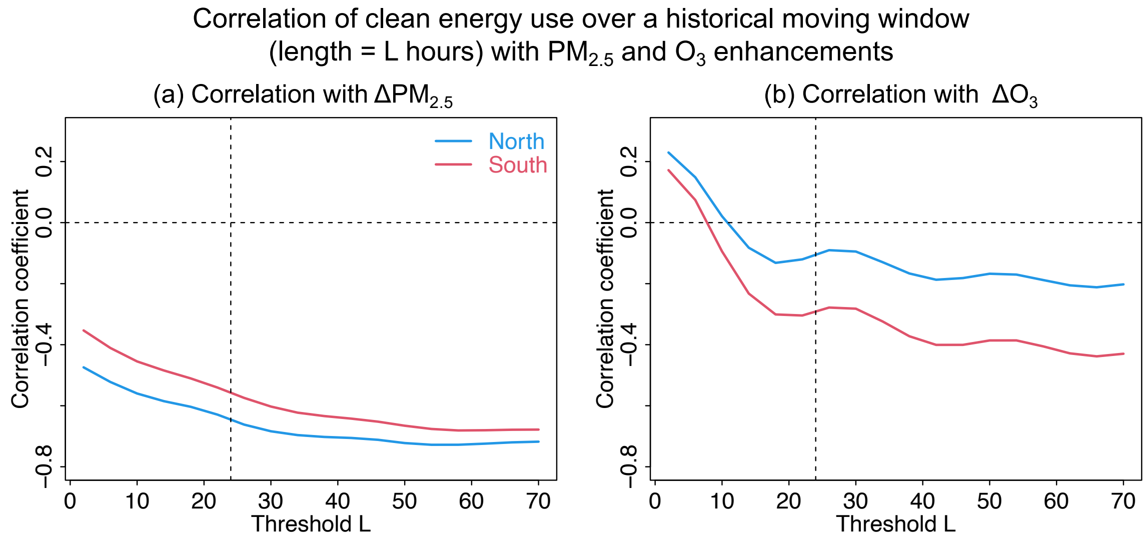

Fig. S8. Correlation between cumulative clean energy use and air quality changes attributable to fossil fuel plant emissions. The clean energy use refers to the electricity use from renewables and nuclear, calculated over a moving historical window of length *L* hours. The changes in $PM_{2.5}$ ($\Delta PM_{2.5}$) and O_3 (ΔO_3) concentrations are defined as differences between the with-fossil scenario and zero-fossil benchmark. (a) Correlation with $\Delta PM_{2.5}$ in the North and South. The vertical dashed line marks $L = 24$ hours, which is the length threshold used in the main text to define renewable energy droughts. The horizontal dashed line indicates a correlation coefficient $r = 0$. (b) Same as (a) but for ΔO_3.

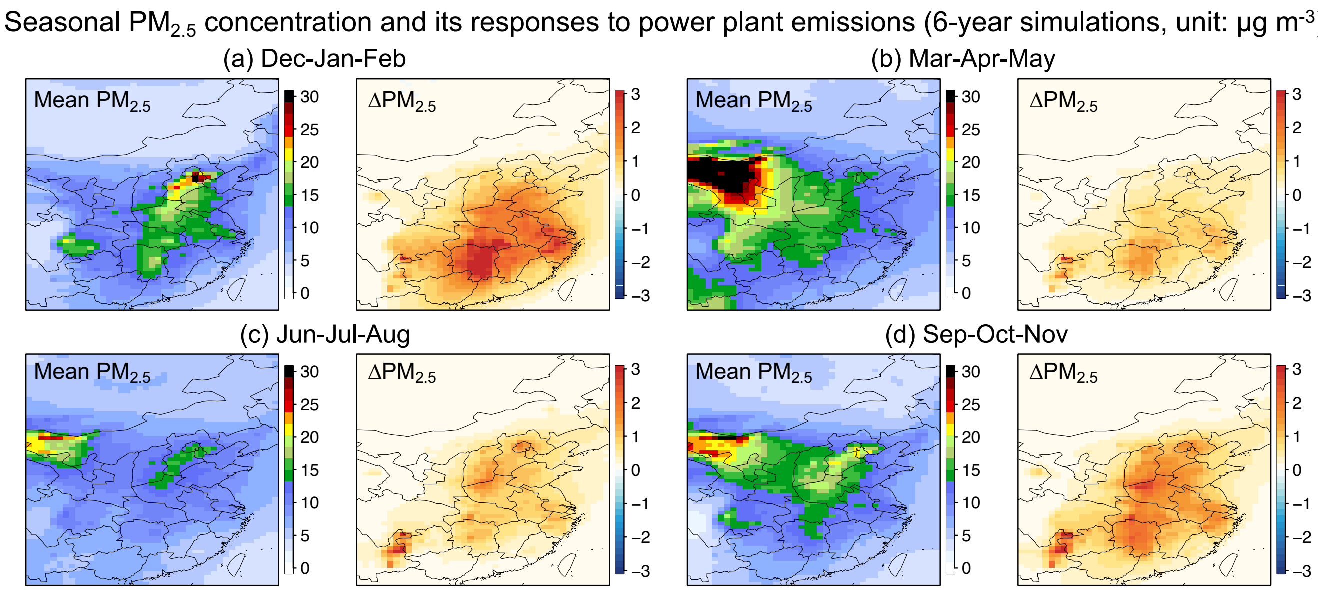

Fig. S9. **Seasonal $PM_{2.5}$ concentrations in 2050 in the zero-fossil benchmark and the relative changes in the representative with-fossil scenario**. The zero-fossil benchmark (the left panel of each seasonal subgroup) set the fossil fuel plant generation to zero. The representative with-fossil scenario (the right panel of each seasonal subgroup) assumes the renewable energy sources contribute 84% of the electricity mix (C2 in Table S1), alongside the implementation of the best end-of-pipe emission controls on power plants. For both panels, MERRA-2 meteorology is applied, along with non-power anthropogenic emissions that align with pollution control targets set for 1.5°C climate goals (see Table S4 for details). Basemaps are adopted from National Catalogue Service for Geographic Information of China (https://www.webmap.cn/main.do?method=index).

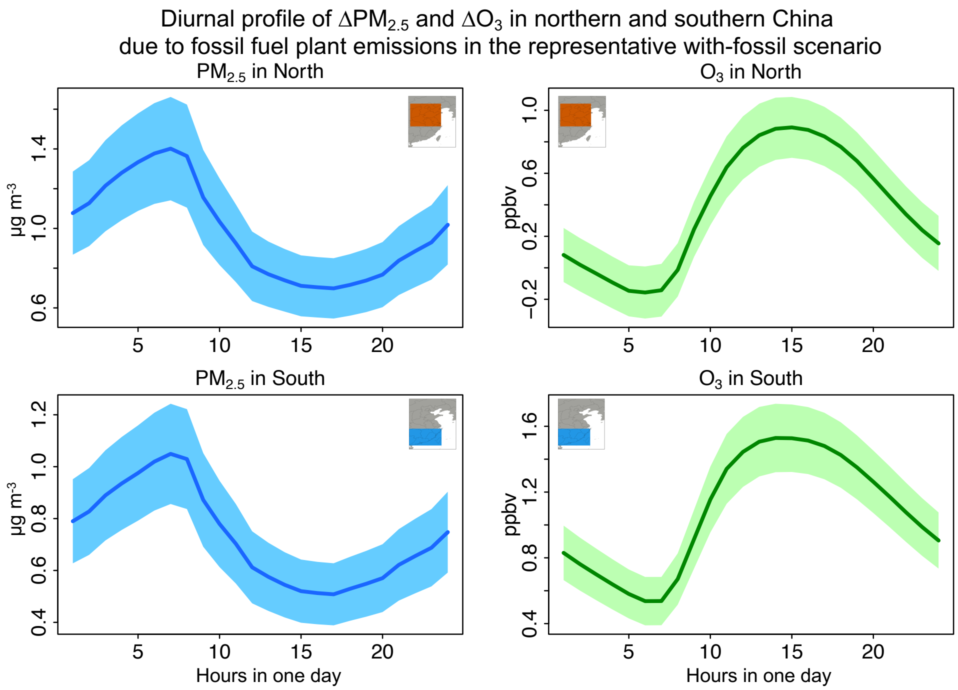

Fig. S10. Multi-year average diurnal changes of O_3 and $PM_{2.5}$ in response to hourly variability of emissions from fossil fuel plants in northern and southern China. Here, the representative with-fossil scenario is from Chen et al.[3](C2 in Table S1), which assumes an 84% renewable penetration rate. Results are averaged across all days, with inset maps showing the geographic domains of northern and southern China. Shared area denoted 95% confidence intervals (N>4000).

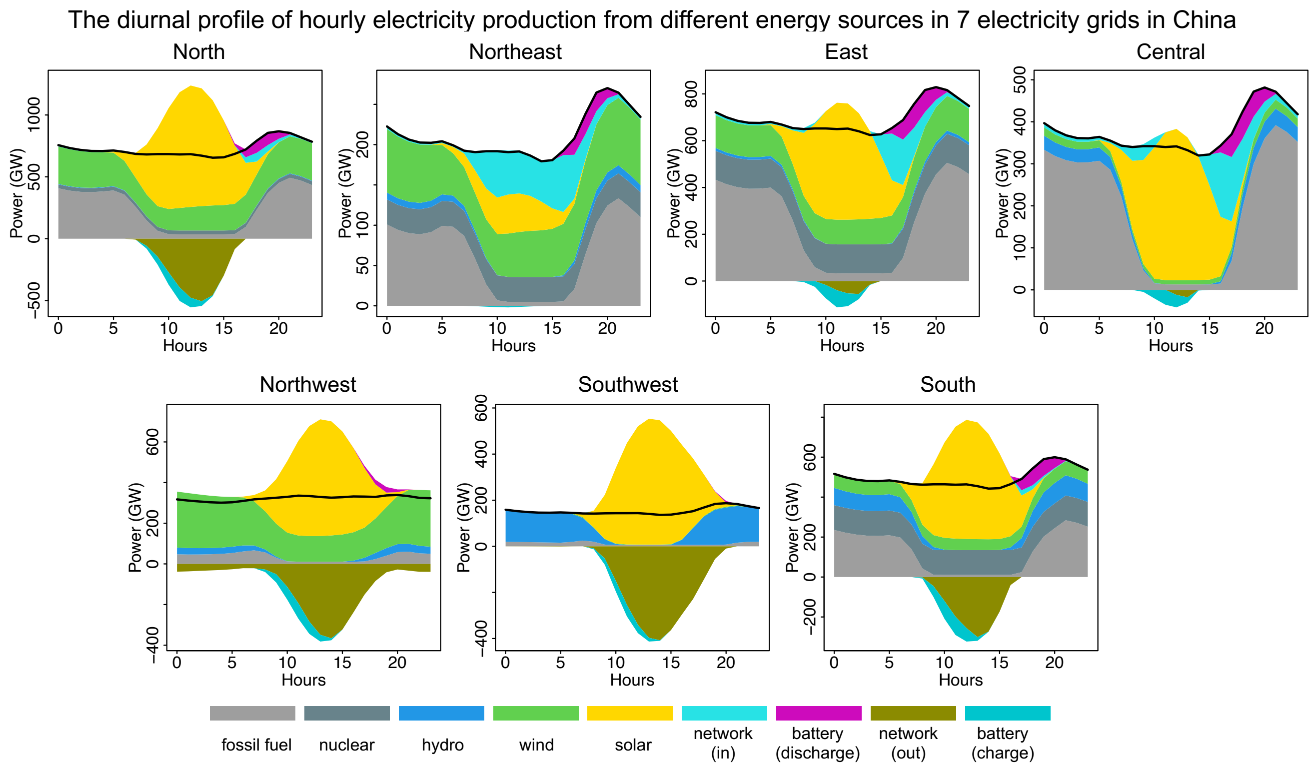

Fig. S11. Annual mean diurnal profile of hourly electricity production from different energy sources in 7 electricity grids in China. Load demands are indicated by the continuous black curves. Negative values imply energy being exported to other regions or used to charge batteries. Here, we use the energy scenario from Chen et al.[3] (C2 in Table S1), which assumes an 84% renewable penetration rate.

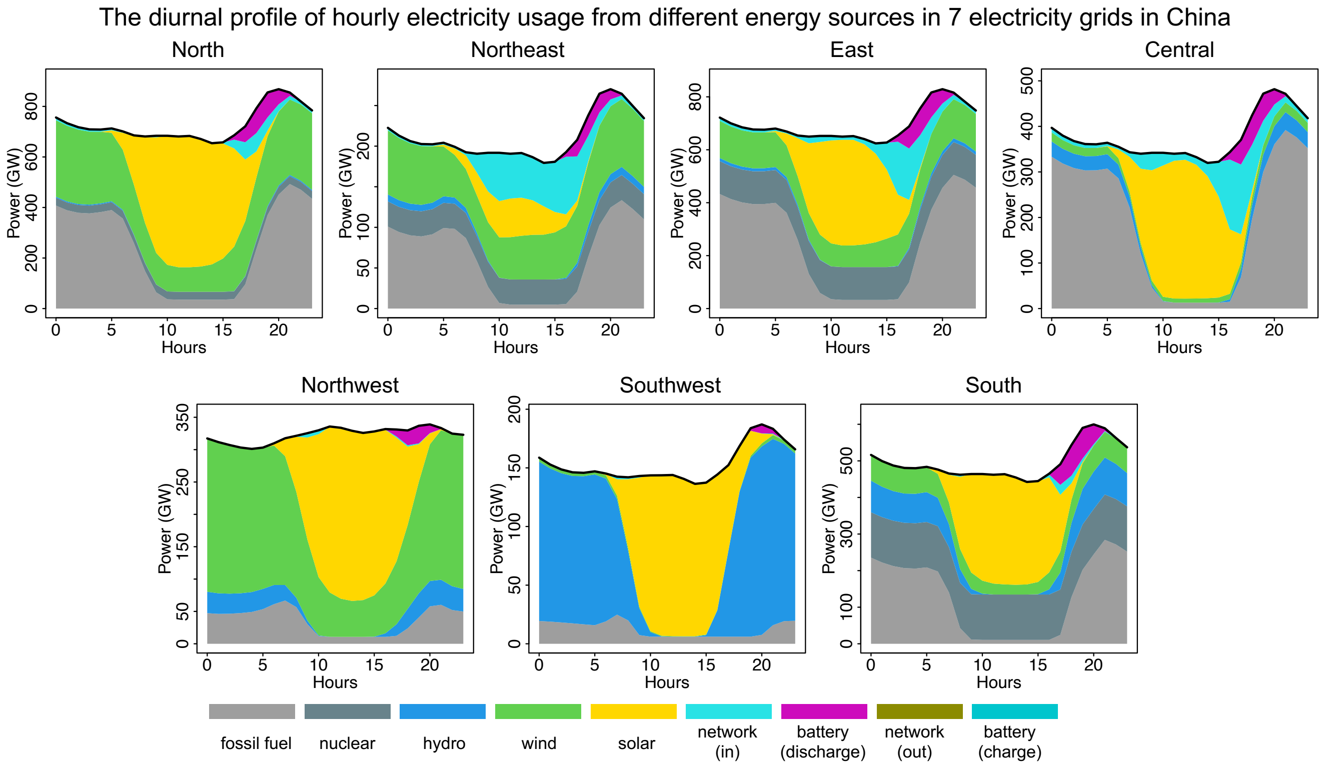

Fig. S12. Annual mean diurnal profile of hourly electricity usage from different energy sources in 7 electricity grids in China. Load demands are indicated by the continuous black curves. Here, we use the energy scenario from Chen et al.[3](C2 in Table S1), which assumes an 84% renewable penetration rate.

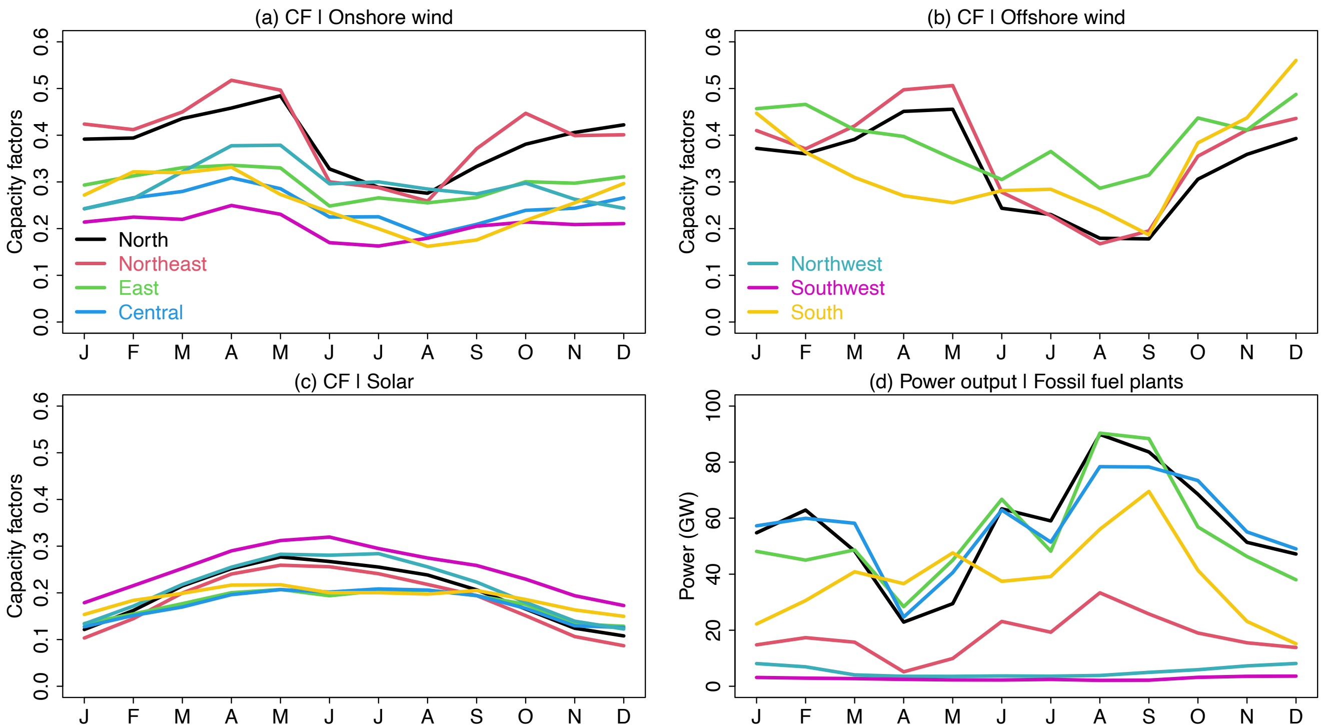

Fig. S13. Monthly mean capacity factors and power output for wind, solar, and fossil fuel generation across China's seven electricity grids (2014–2019). Panels show monthly mean capacity factors for (a) onshore wind, (b) offshore wind, and (c) solar, along with (d) fossil fuel power output. Wind power curves are from the onshore General Electric 2.5MW and the offshore MHI Vestas V164-8.0MW wind turbines (see details in Methods).

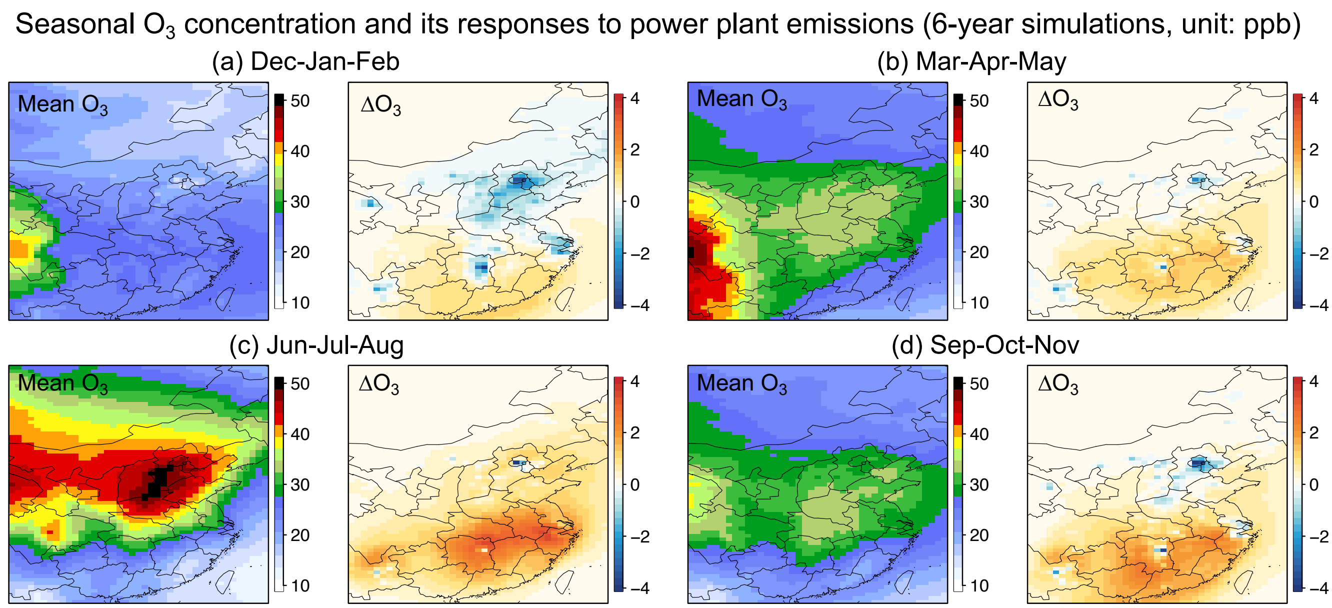

Fig. S14. Same as Fig. S9, but for average ozone concentrations. Basemaps are adopted from National Catalogue Service for Geographic Information of China (https://www.webmap.cn/main.do?method=index).

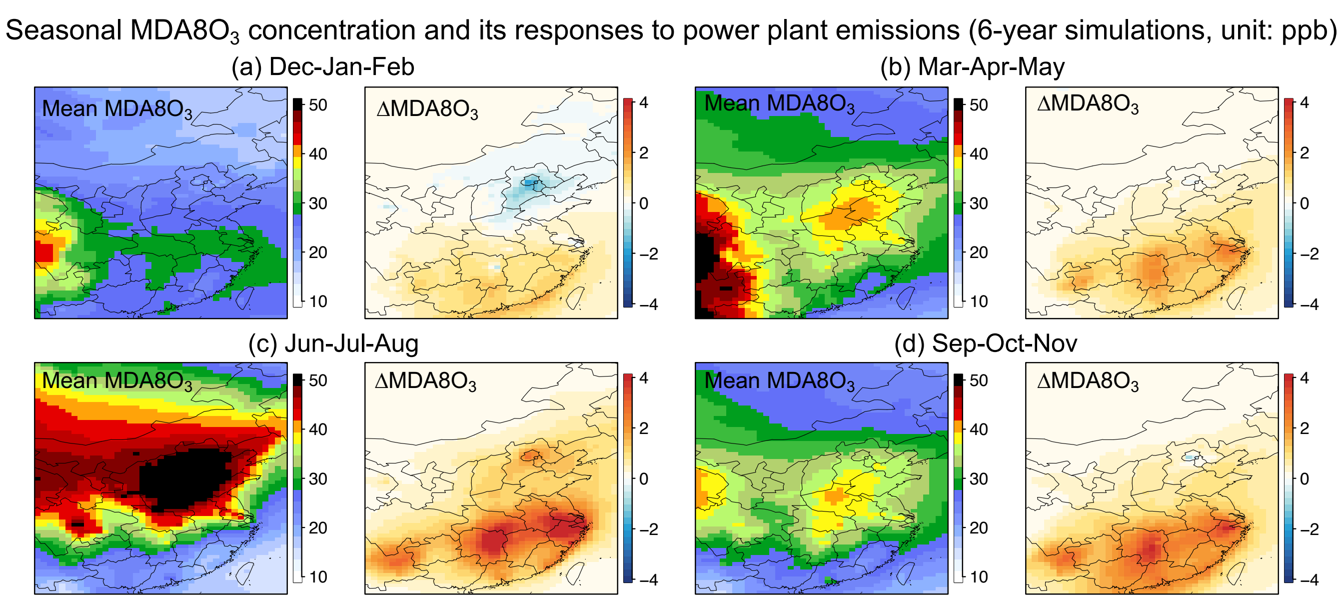

Fig. S15. Same as Fig. S9, but for daily maximum 8-hour average (MDA8) ozone concentrations. Basemaps are adopted from National Catalogue Service for Geographic Information of China (https://www.webmap.cn/main.do?method=index).

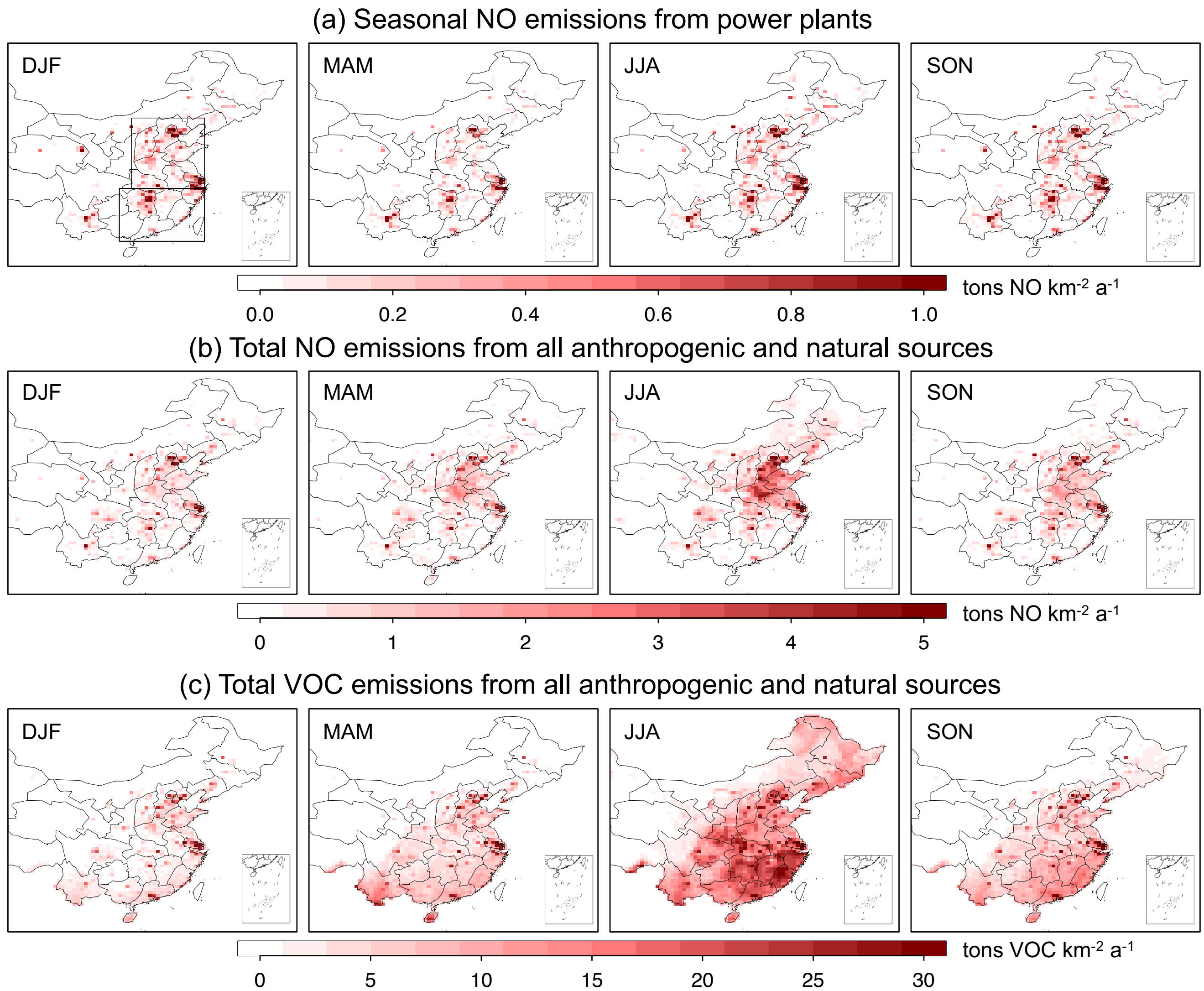

Fig. S16. Seasonal distribution of NO and VOC emissions in China. (a) Seasonal mean NO emission intensity from fossil fuel plants under the with-fossil scenario of Chen et al.[3](C2 in Table S1), which assumes an 84% renewable penetration rate. (b) Seasonal mean total NO emissions from all anthropogenic and natural sources. Anthropogenic NO emissions are taken from the DPEC "ambitious-pollution-1.5 °C-goal" scenario for 2050[16], while additional sources include cropland and natural soil emissions[17]. (c) Same as(b), but for VOC emissions, including both anthropogenic and biogenic sources[18]. In this figure, NO_x emissions are expressed as NO, which can be converted to a NO_2-equivalent mass by applying the molecular weight ratio of 46/30. Basemaps are adopted from National Catalogue Service for Geographic Information of China (https://www.webmap.cn/main.do?method=index).

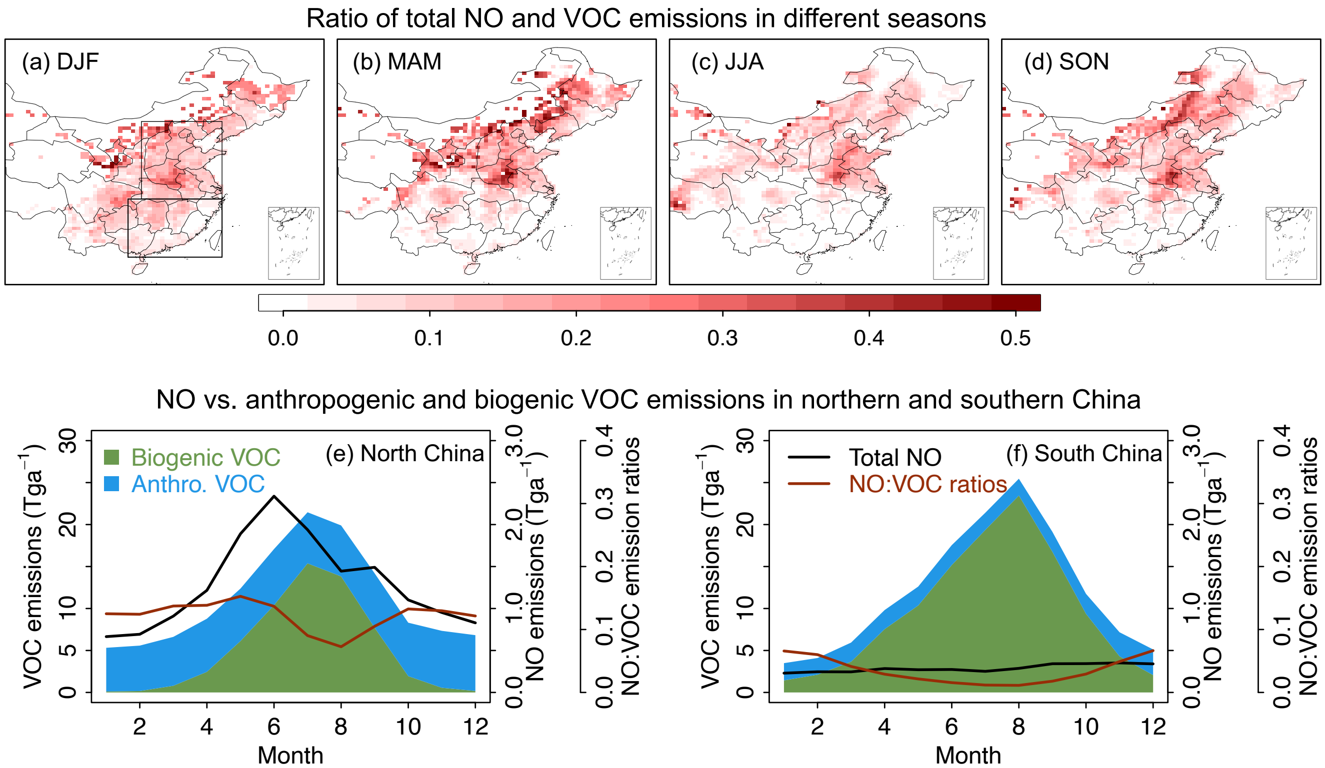

Fig. S17. Seasonal ratios and monthly time series of NO and VOC emissions in China. (a–d) Seasonal ratios of total NO to VOC emissions, where total emissions include both anthropogenic and biogenic sources. (e–f) Monthly time series of total NO and VOC emissions (anthropogenic + biogenic) aggregated over northern and southern China. Red lines indicate the corresponding NO/VOC emission ratios. In this figure, NO_x emissions are expressed as NO, which can be converted to a NO_2-equivalent mass by applying the molecular weight ratio of 46/30. Basemaps are adopted from National Catalogue Service for Geographic Information of China (https://www.webmap.cn/main.do?method=index).

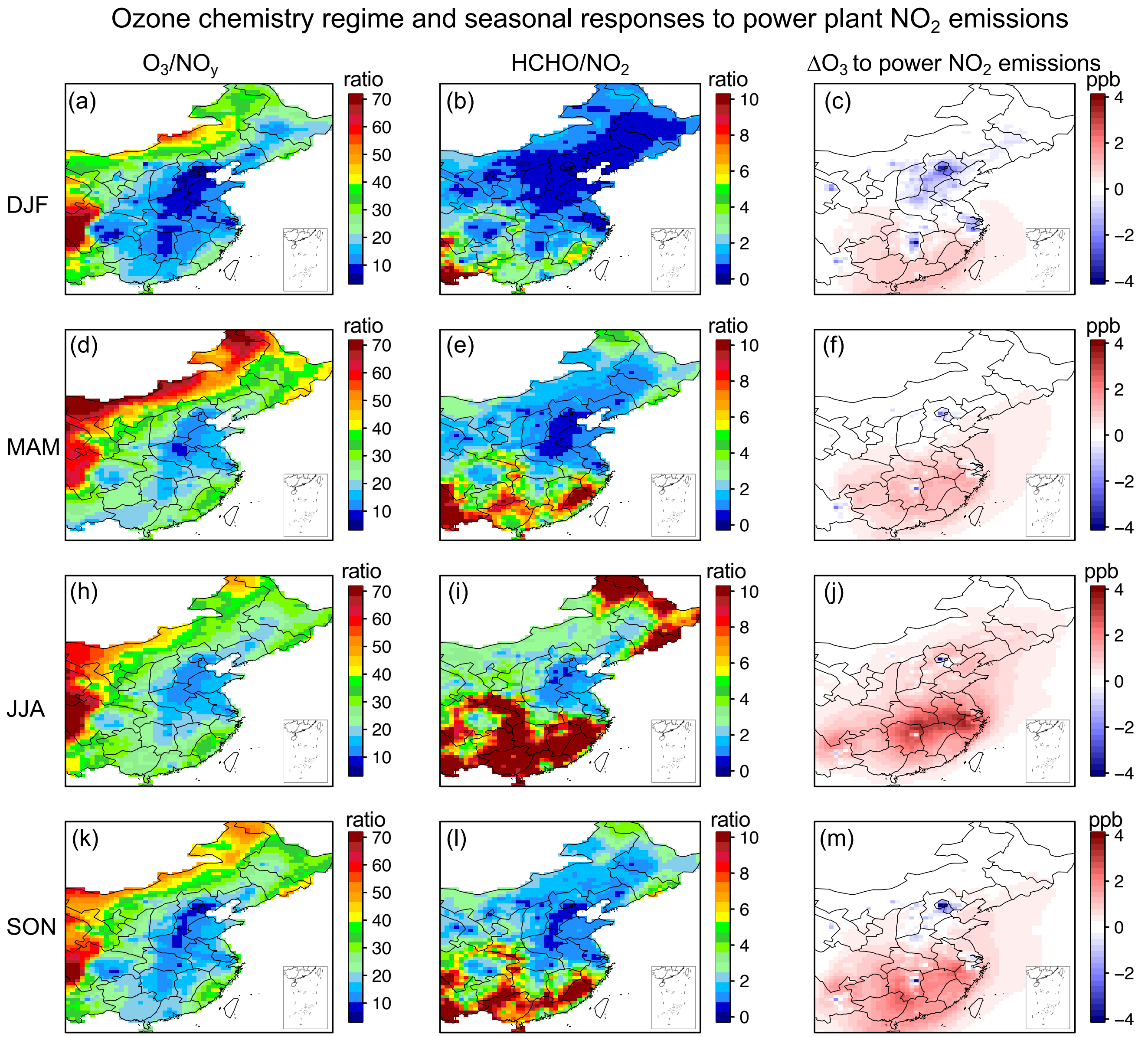

Fig. S18. Seasonal indicators of ozone chemical regimes and responses to fossil fuel emissions. (left column) Seasonal distributions of boundary-layer O_3/NO_y ratios, where lower values indicate a greater propensity for VOC-limited regimes[19]. Here, NO_y refers to the sum of NO_x and its oxidation products. (middle column) Seasonal distributions of $HCHO/NO_2$ ratios, with lower values likewise indicating VOC-limited conditions[19,20]. (right column) Seasonal O_3 concentration responses to fossil fuel power plant emissions (consistent with Fig. S14). Negative responses indicate ozone titration by increased NO_x or a VOC-limited chemical regime. Basemaps are adopted from National Catalogue Service for Geographic Information of China (https://www.webmap.cn/main.do?method=index).

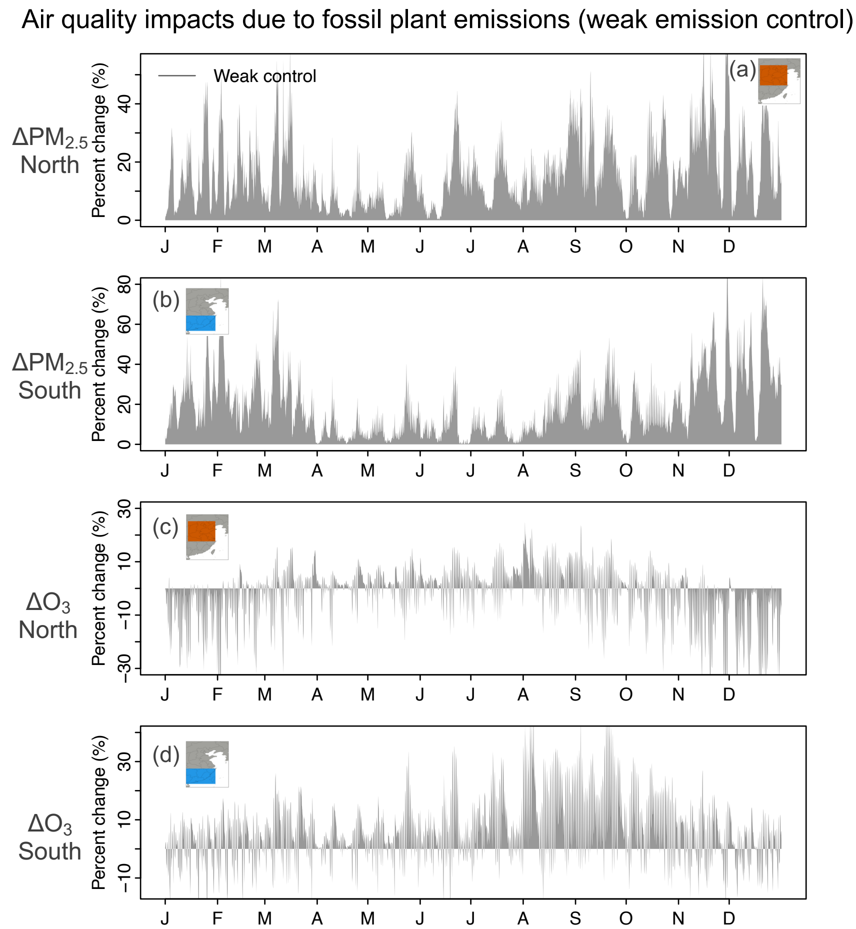

Fig. S19. Hourly relative changes of $PM_{2.5}$ and O_3 levels in northern and southern China arising from fossil fuel plane emissions. This figure is analogous to Fig. 2 but assumes weak end-of-pipe emission control policies for fossil fuel power plants (see Table S2 for the emission factors with weak control policies).

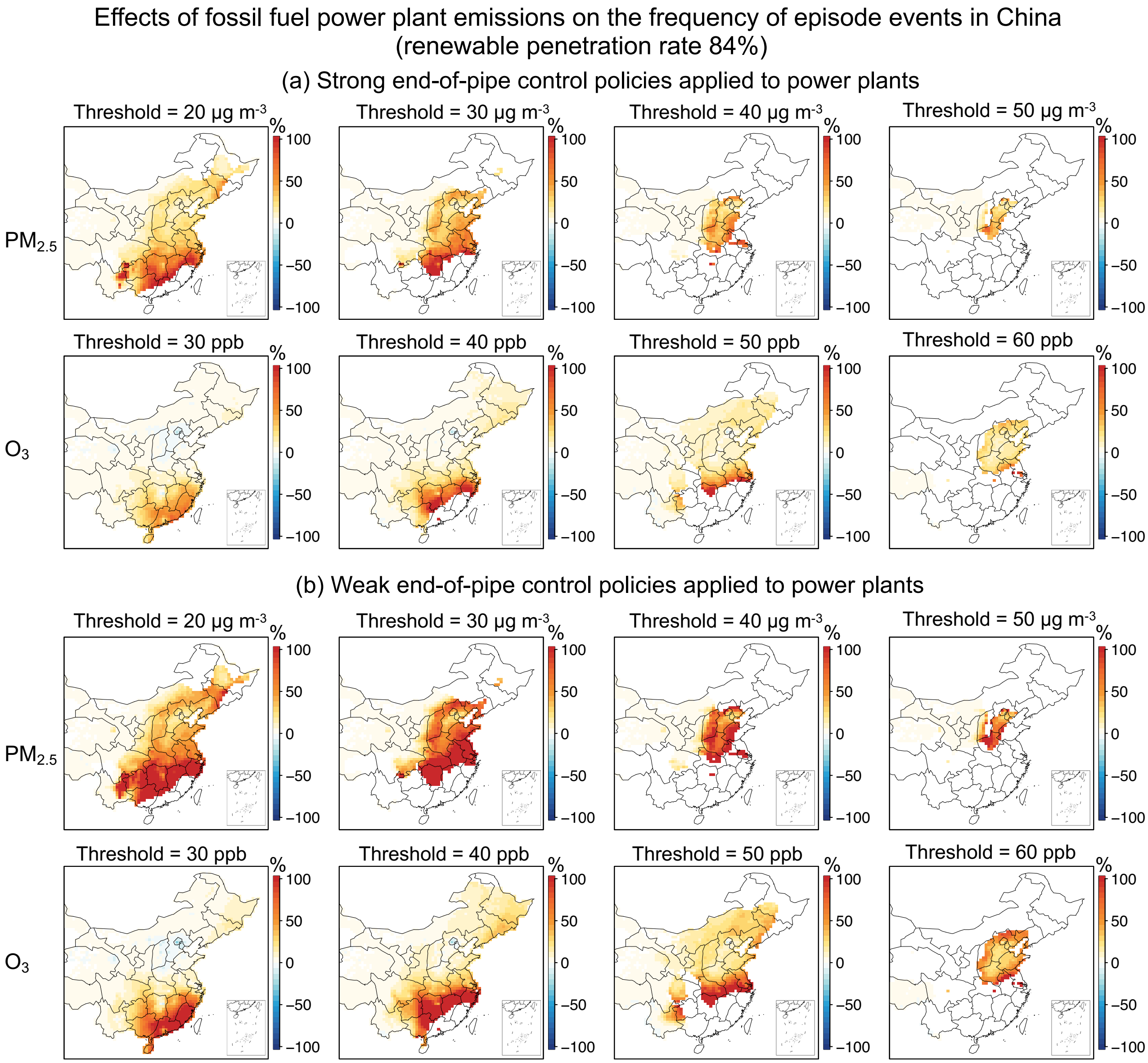

Fig. S20. **Effects of fossil fuel plant emissions on the frequency of extreme pollution hours in China in 2050, relative to zero-fossil benchmark.** Here, we define the extreme pollution hours with different thresholds for $PM_{2.5}$ and O_3. We assume a stringent and a weaker end-of-pipe control policies applied to power plants (see Table S2 for the emission factors), as shown in panel (a) and (b). Here, we use the energy scenario from Chen et al.[21](C2 in Table S1), which assumes an 84% renewable penetration rate. Gridcells with fewer than 20 annual extreme pollution hours are shown in white. Basemaps are adopted from National Catalogue Service for Geographic Information of China (https://www.webmap.cn/main.do?method=index).

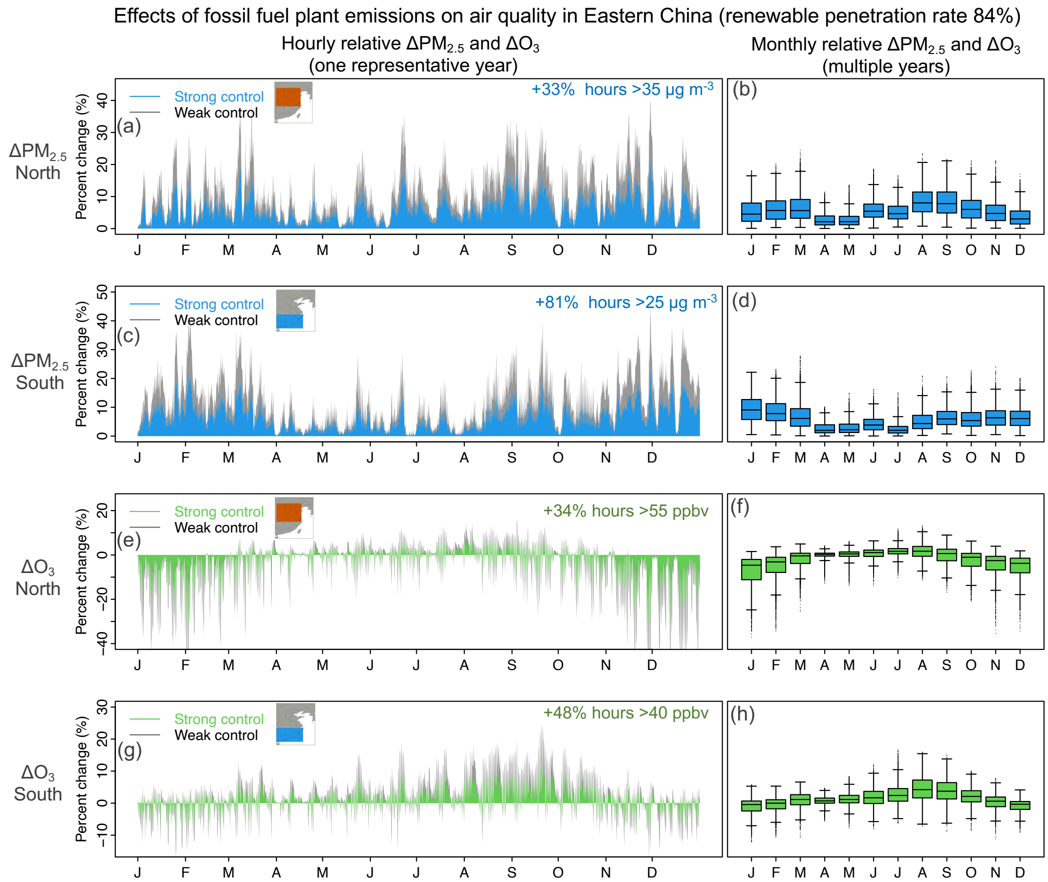

Fig. S21. Same as Fig. 2, but non-power emissions aligned with the 2°C goals. See Table S4 for different selections of these non-power anthropogenic emissions.

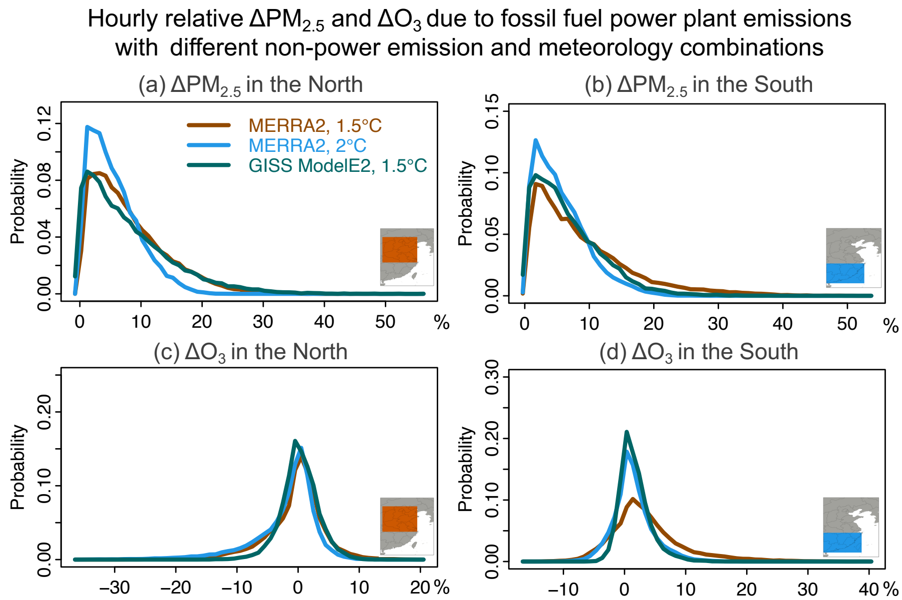

Fig. S22. Distribution of relative changes of air pollutants using different emission and meteorological datasets. For meteorology, MERRA2 for the 2010s and GISS ModelE2 for the 2050s are used to drive GEOS-Chem simulations at a resolution of 50km. For non-power plant anthropogenic emissions, we use the two inventories from the DPEC inventory, such as 'ambitious-pollution-1.5℃-goal' and 'ambitious-pollution-2℃-goal' (Table S4). We assume the implementation of a stringent emissions control policy for power plants (Table S2).

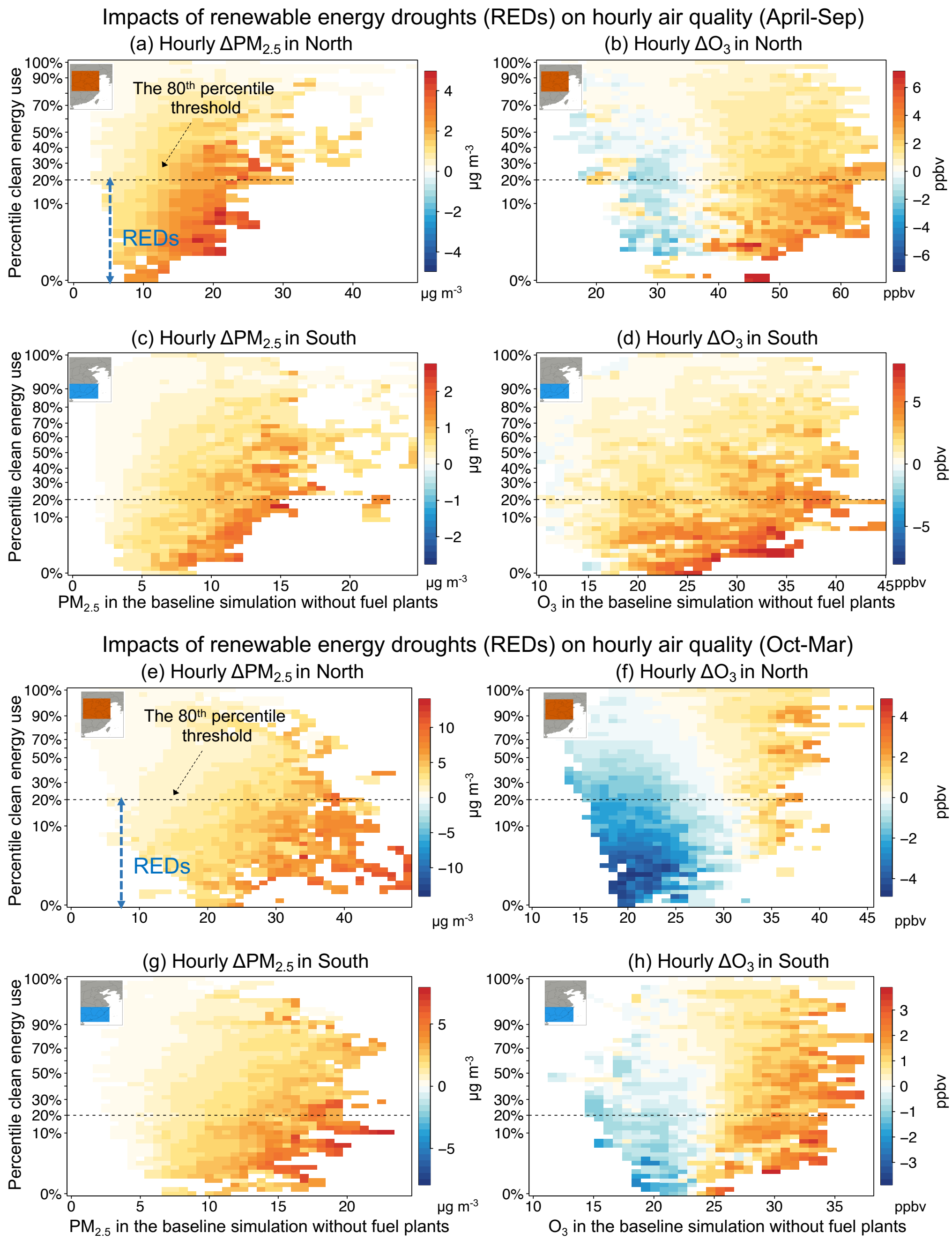

Fig. S23. Same as Fig. 3 but for warm (a-d) and cold (e-h) seasons. Here, the warm season refers to April-September, and the cold season refers to October-March. Basemaps are adopted from National Catalogue Service for Geographic Information of China (https://www.webmap.cn/main.do?method=index).

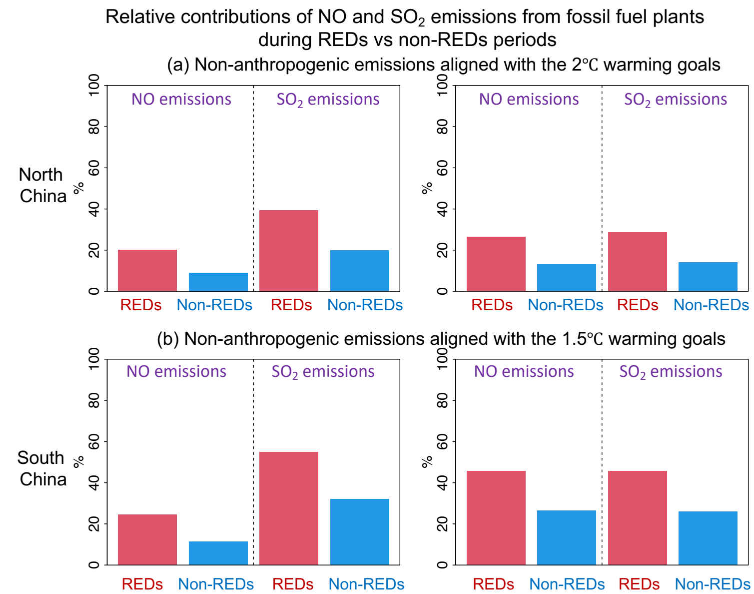

Fig. S24. Fossil fuel plant contributions to total NO_x and SO_2 emissions during renewable energy droughts (REDs, red) versus non-RED periods (blue). Values represent percentage shares of total emissions. The emission scenario here is consistent with that in Fig. 1-4.

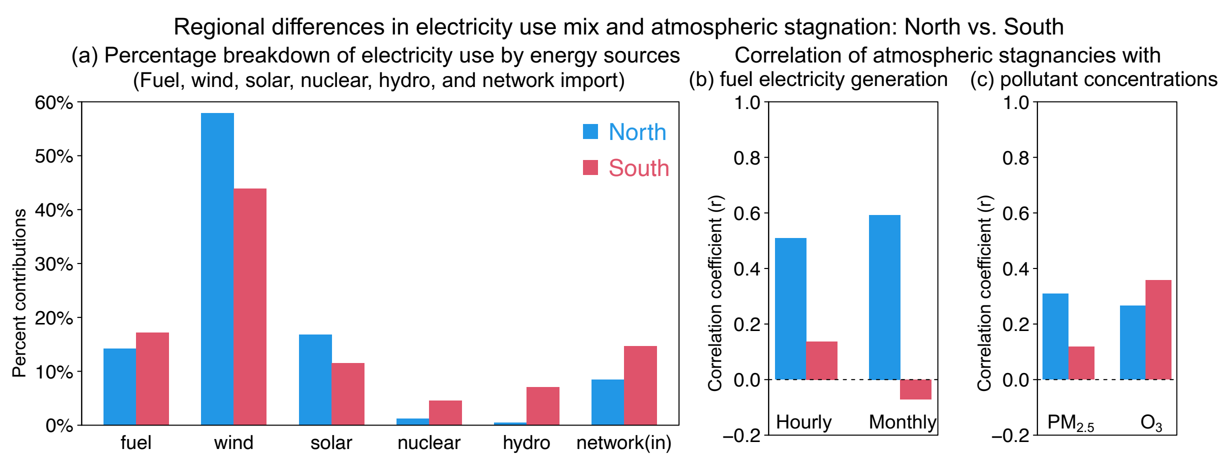

Fig. S25. Regional differences in electricity use mix and impacts of atmospheric stagnation. (a) Percentage contribution of electricity sources — fuel plants, wind (onshore + offshore), solar, nuclear, hydro, and network imports —in northern and southern China. (b) Correlation between atmospheric stagnation and cumulative fuel plant electricity generation over the past 24 hours, calculated hourly and monthly. (c) Correlation coefficients of atmospheric stagnation with $PM_{2.5}$ and O_3 under the baseline scenario. The definition of atmospheric stagnation is defined in Text S3.

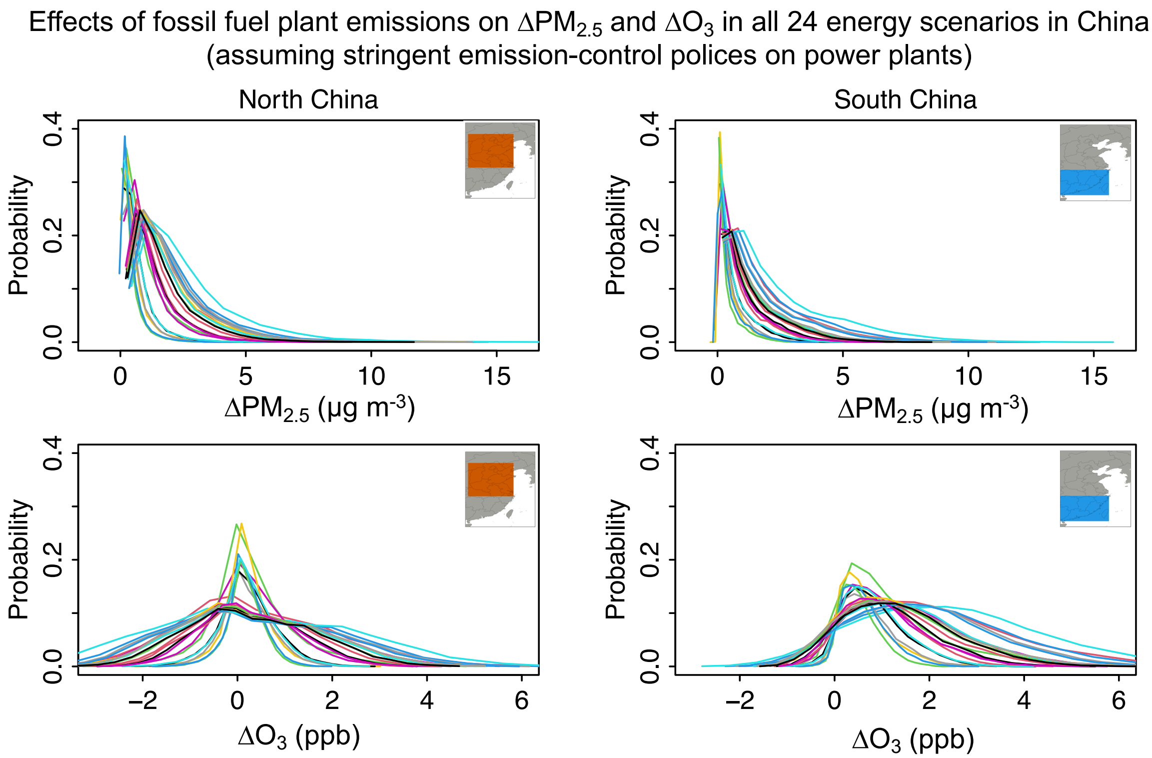

Fig. S26. **Effects of fossil fuel plant emissions on air pollutants ($PM_{2.5}$ and O_3) concentrations in 24 energy projections in northern and southern China**. The inset maps denote the locations of northern and southern China domains. These 24 energy projections can be found in Table S1. We assume a stringent end-of-pipe control policies applied to power plants (see Table S2 for the emission factors). See Text S4 for how we extrapolate hourly O_3 and $PM_{2.5}$ concentrations to all energy scenarios based on GEOS-Chem simulations.

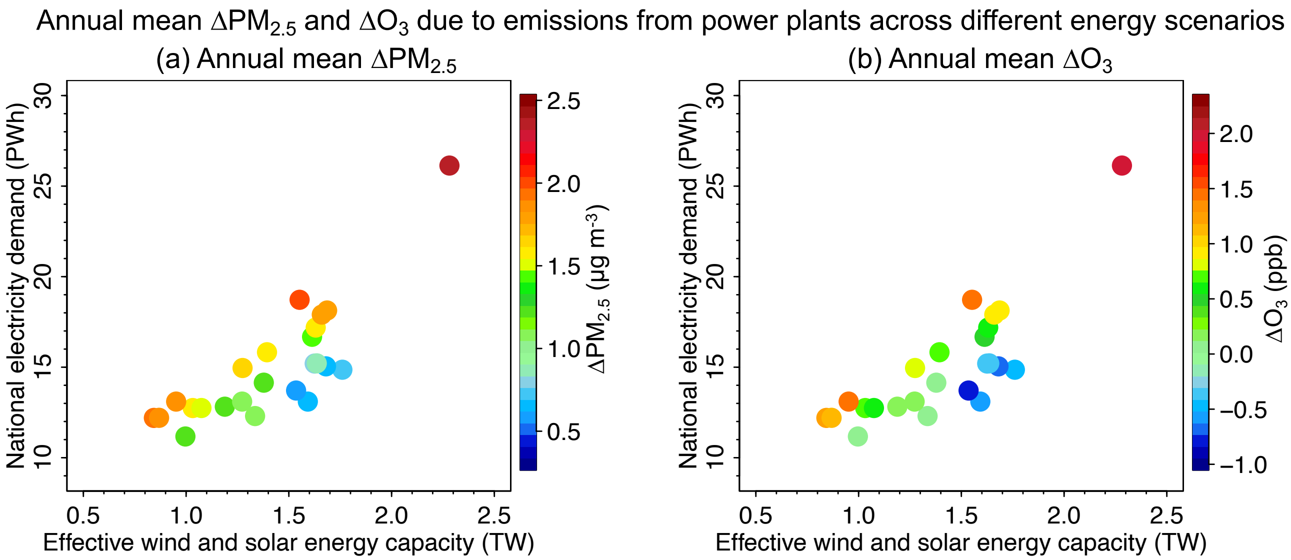

Fig. S27. **Relationship of annual mean $\Delta PM_{2.5}$ and ΔO_3 in 24 energy scenarios with effective clean energy (wind + solar) capacity and national electricity demand**. These 24 energy projections can be found in Table S1. Different colors refer to annual mean $\Delta PM_{2.5}$ and ΔO_3, representing air quality impacts from fossil fuel plant emissions. See Text S4 for how we extrapolate hourly O_3 and $PM_{2.5}$ concentrations to all energy scenarios based on GEOS-Chem simulations.

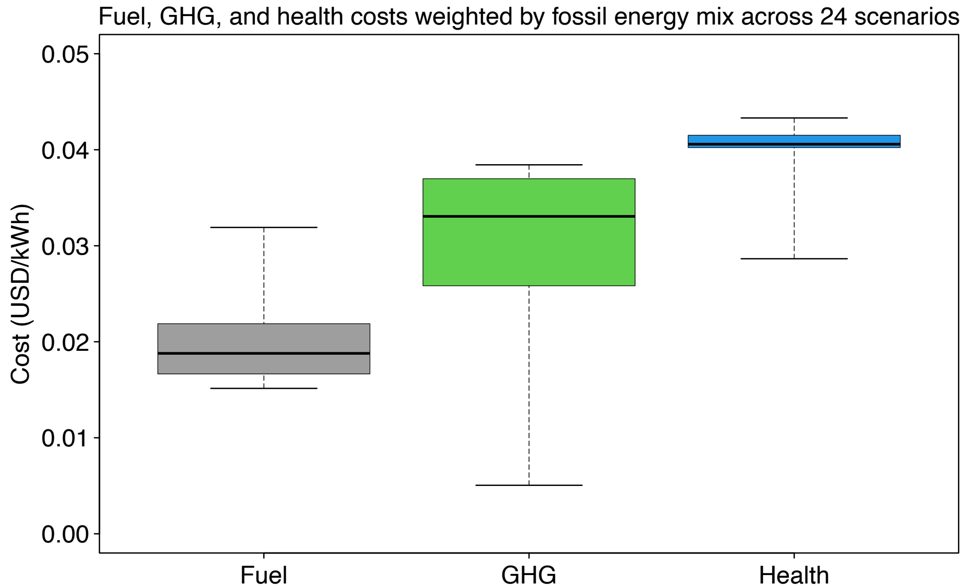

Fig. S28. **Distribution of fossil fuel, greenhouse gas (GHG), and health costs per every kWh electricity generation from fossil fuel plants across 24 energy scenarios**. The analysis includes coal, natural gas, and biomass power plants. While the unit costs for each fuel type are fixed across scenarios (see Table S7 for details), the integrated costs, which are weighted by each scenario's fossil energy generation, vary across the 24 energy scenarios. Specifically, within each scenario, the integrated cost for fuel consumption is calculated as electricity-generation–weighted averages across fossil fuel types. A similar approach is also applied to greenhouse gas costs (based on CO_2 emissions) and health costs. In the boxplots, the central line denotes the median, the hinges correspond to the 25th and 75th percentiles, and the whiskers extend to the minimum and maximum values across the 24 energy scenarios.

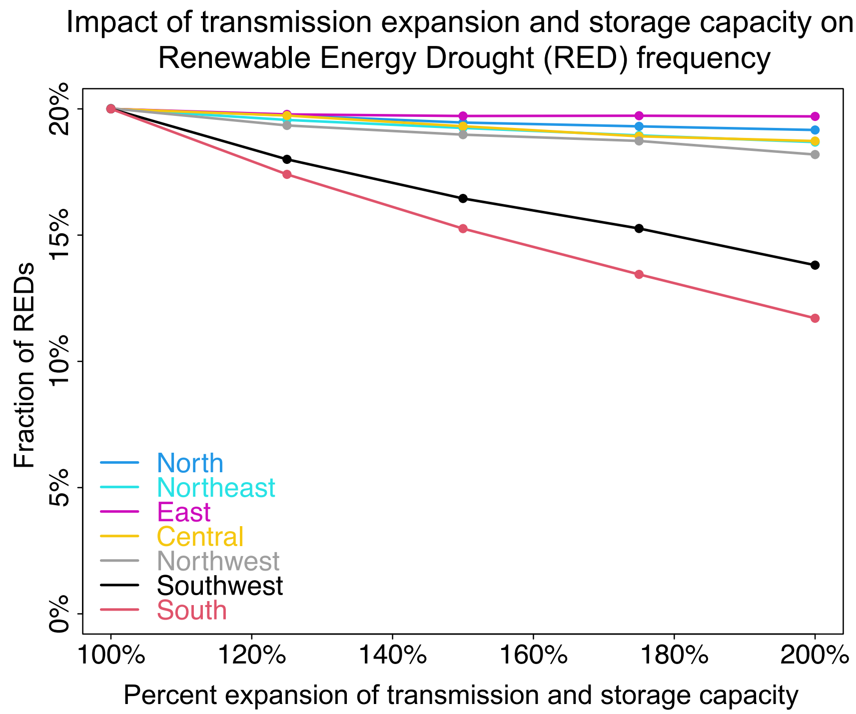

Fig. S29. Changes in renewable energy drought (RED) frequency with expanded storage and transmission capacity across regional electricity grids. In the representative with-fossil scenario, where fossil fuel power plants supply 16% of total electricity demand, transmission and storage capacities are scaled from 100% to 200% in 20% increments. The electricity system model developed in this study (details in Text S1) is used to simulate electricity generation from different energy sources, from which we calculate the fraction of hours classified as renewable energy droughts (REDs) across the seven regional electricity grids. The corresponding deployment shares of different energy sources in each grid are shown in Fig. S33.

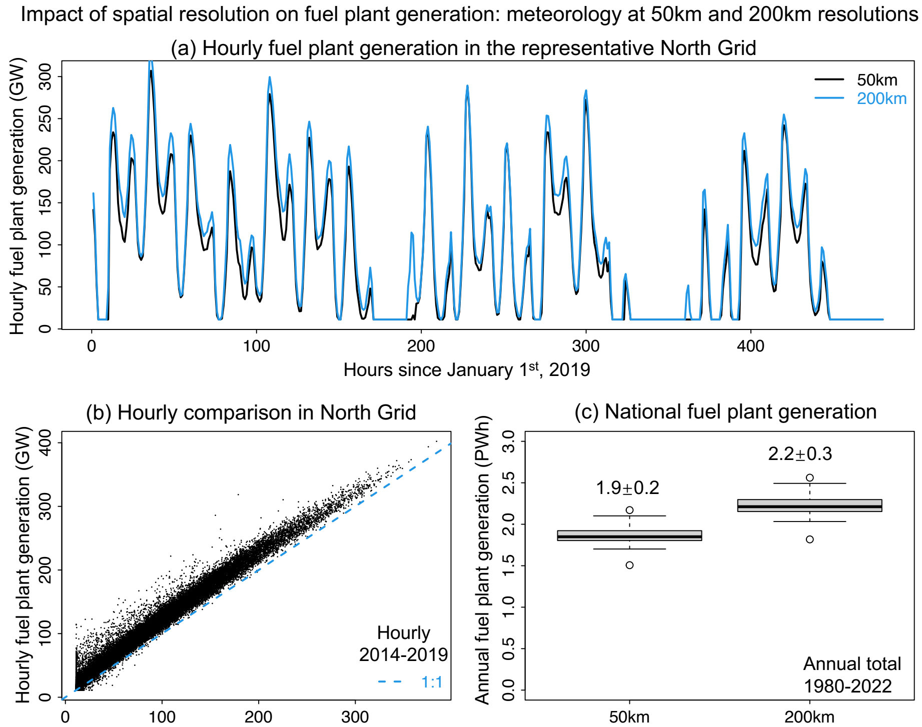

Fig. S30. Impact of meteorological spatial resolution (50 km vs. 200 km) on fossil fuel plant generation. Meteorological data (wind and solar) are regridded from 0.5°×0.625° (~50 km) to a coarse resolution 2°×5° (~200 km), and input into the electricity model with identical parameters. (a) Time series of hourly fossil fuel plant emissions for the first 500 hours of 2019 in the North Electricity Grid, comparing results from the two spatial resolutions. The correlation coefficient (*r*) between the two time-series exceeds 0.98. (b) Scatterplot comparing hourly fossil fuel plant emissions across all hours (2014–2019). (c) National fossil fuel plant generation derived from meteorological data at both resolutions. In the boxplots, the central line denotes the median, hinges correspond to the 25th and 75th percentiles, whiskers extend to the 2.5th and 97.5th percentiles, and points beyond the whiskers represent outliers. These statistics are based on annual total generation over 44 years (N = 44).

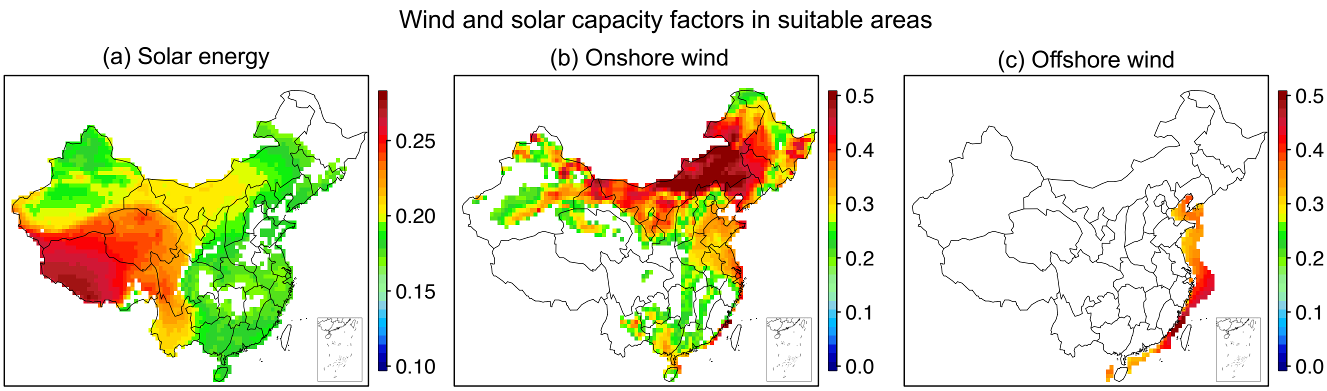

Fig. S31. **Capacity factors for onshore wind, offshore wind and solar energy**. The CFs are calculated using MERRA2 reanalysis data. White gridboxes indicate areas where either renewable installation is not suitable or the CFs are too low. See Table S11 for the selection of suitable areas. Basemaps are adopted from National Catalogue Service for Geographic Information of China (https://www.webmap.cn/main.do?method=index).

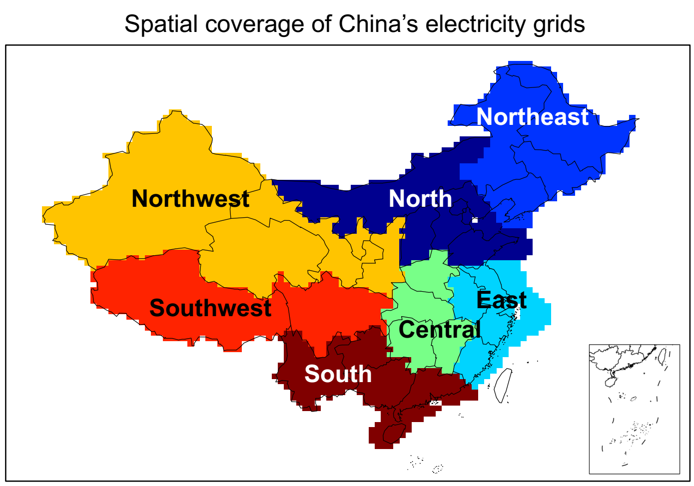

Fig. S32. **The seven electricity grids from the State Grid Corporation of China** (SGCC[2]). Offshore gridcells suitable for wind turbines are also integrated into the adjacent electricity grids. See Methods for more details. Basemaps are adopted from National Catalogue Service for Geographic Information of China (https://www.webmap.cn/main.do?method=index).

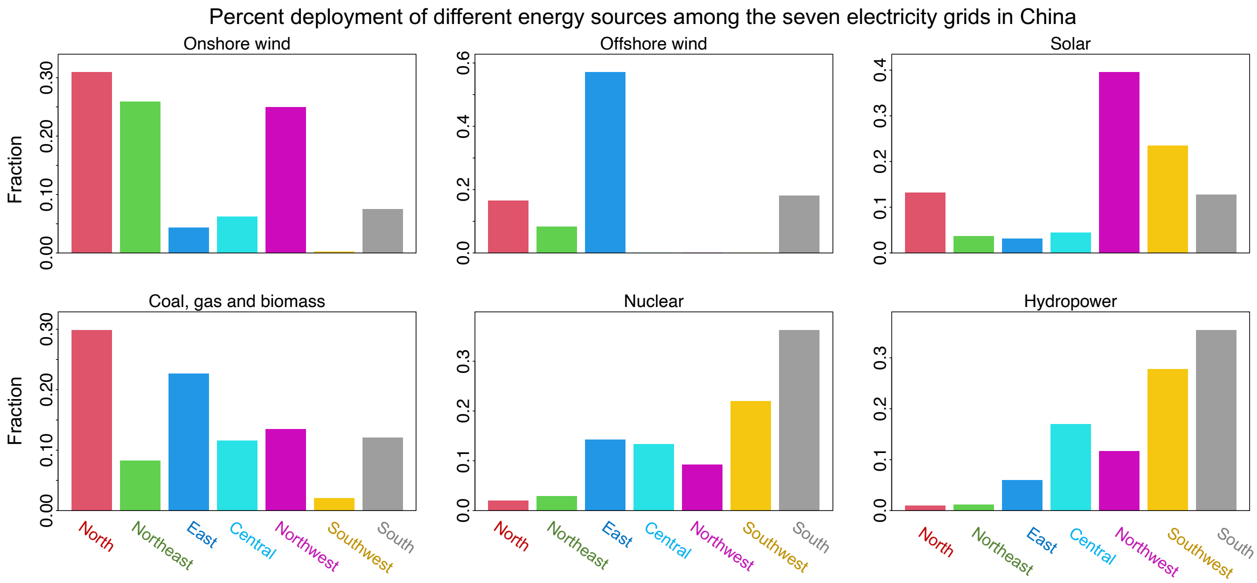

Fig. S33. Percent deployment of different energy sources among the seven electricity grids. This data is sourced from the State Grid Corporation of China (SGCC[2]).

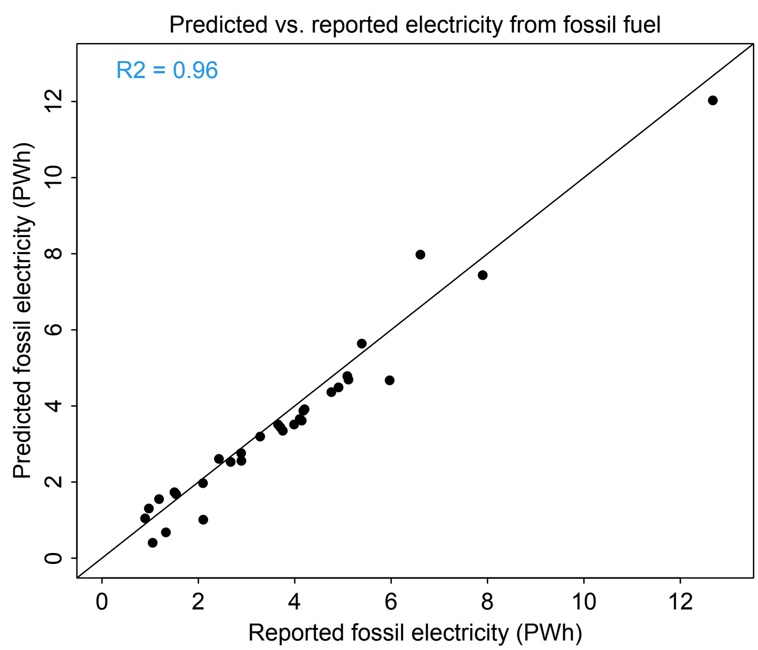

Fig. S34. Comparison of the annual electricity generation from fossil fuel power plants in our electricity system model with reported values from 24 energy projections (Table S1). The correlation coefficient is 0.96 with no systematic bias.

Table S1. **Renewable energy capacity and national electricity demand collected from previous studies**, all targeting the 1.5°C and 2°C warming goals or with high renewable penetration. More details can be found in supplementary Dataset S1. Note that C0 denotes the zero-fossil benchmark in which fossil fuel plant generation is set to zero, while C2 represents the representative with-fossil scenario (shown in Fig. 1–4 of the main text)

	References	**Category**	**National Electricity demand (PWh)**	**Effective wind and solar capacity# (GW)**	**Electricity generation from fuel-based plants (coal+gas+biomass, PWh)**	**Percentage of fuel-based electricity in total production**	**How we obtain the air quality responses of this energy scenario (A) GEOS-Chem (B) Statistical extrapolation**	**Description**
C0		No fuel plant emissions					A (The **zero-fossil** scenario)	This scenario is not intended to represent an actual future projection, but rather provides a baseline for comparative analysis.
C1	Chen et al.[3]	2050-60%	13.10	747	4.76	36%	A	Near neutrality
C2	Chen et al.[3]	2050-80%	13.10	1077	2.10	16%	A (The **representative** with-fossil scenario)	Carbon neutrality
C3	Wang et al.[22]	2050-Optimal	18.72	1078	5.39	29%	B	Carbon neutrality
C4	Wang et al.[22]	2060-Optimal	26.13	1720	6.61	25%	A	Carbon neutrality
C5	Zhuo et al.[23]	2050-NDC	12.30	911	2.10	17%	B	Nationally Determined Contribution
C6	Zhuo et al.[23]	2050-2.0°C	13.10	1136	1.05	8%	B	2°C goal
C7	Zhuo et al.[23]	2050-Carbon Neutrality	14.86	1309	1.33	9%	B	Carbon neutrality
C8	China Energy Foundation[24]	2050-high renewables	15.20	1103	1.50	10%	B	Carbon neutrality (high renewable penetrations)
C9	Zhang and Chen[25]	2050-NDC	11.17	556	2.89	26%	A	Include NDC and current lauched policies
C10	Zhang and Chen[25]	2050-PEAK20	13.71	1088	0.90	7%	B	Early action scenario, taking ambitious climate action from 2021
C11	Zhang and Chen[25]	2050-PEAK25	15.04	1232	0.97	6%	B	Early action scenario, taking ambitious climate action from 2026
C12	Zhang and Chen[25]	2050-PEAK30	15.21	1186	1.54	10%	B	Early action scenario, taking ambitious climate action from 2031
C13	Fan et al.[26]	2050	14.95	771	4.14	28%	B	Near carbon neutrality
C14	Fan et al.[26]	2060	15.82	850	3.99	25%	B	Carbon neutrality
C15	Ou et al.[27]	GP_CurPol_T46 (2050)	12.20	494	5.11	42%	B	Current Policies scenarios. Expected to lead to 2.7 °C by 2100.
C16	Ou et al.[27]	GP_Glasgow (2050)	12.82	673	2.89	23%	B	Pledges based on2022 COP26 Glasgow Summit, likely taking the world closer to below 2°C in 2100
C17	Ou et al.[27]	GP_GlasgowP (2050)	16.68	845	3.28	20%	B	Expands mid-century strategy pledges to net-zero for all countries and regions.

C18	Ou et al.[27]	GP_GlasgowPP (2050)	17.19	846	3.66	21%	B	Between national mid-century strategies and the 1.5/2 °C global scenarios.
C19	Ou et al.[27]	GP_NDC2030_T46 (2050)	12.20	509	4.91	40%	B	NDCs until 2030, and then reduces emissions typically in line with a globally 2°C by 2100.
C20	Ou et al.[27]	GP_CurPol_T46 (2060)	12.74	589	4.10	32%	B	Current Policies scenarios. Expected to lead to 2.7 °C by 2100.
C21	Ou et al.[27]	GP_Glasgow (2060)	14.14	742	2.67	19%	B	Pledges based on2022 COP26 Glasgow Summit, likely taking the world closer to below 2°C in 2100
C22	Ou et al.[27]	GP_GlasgowP (2060)	17.90	787	4.18	23%	B	Expands mid-century strategy pledges to net-zero for all countries and regions.
C23	Ou et al.[27]	GP_GlasgowPP (2060)	18.13	786	4.20	23%	B	Between national mid-century strategies and the 1.5/2 °C global scenarios.
C24	Ou et al.[27]	GP_NDC2030_T46 (2060)	12.74	613	3.75	29%	B	NDCs until 2030, and then reduces emissions typically in line with a globally 2°C by 2100.

[#] Here effective wind and solar capacity is estimated by dividing their electricity generation by the total number of hours in a year.

Table S2. **Emission factors for fossil fuel power plants in 2050**, obtained from the Dynamic Projection model for Emissions in China (DPEC) inventory [1,8,15]. For coal plants, we assume the deployment of strong and weak end-of-pipe emission control technologies [8].

	Coal | biomass[†]		Gas $g\ kWh^{-1}$
	Strong control ($g\ kWh^{-1}$)	Weak control ($g\ kWh^{-1}$)	
NO_2	0.27	0.52	0.23
SO_2	0.15	0.26	0
$PM_{2.5}$	0.02	0.04	0

[†]Due to the lack of reported emission factors for biomass power plants, we assume they have the same emission factors as coal-fired plants.

Table S3. List of CMIP6 climate models and their corresponding ensemble members (realizations) analyzed in this study for the SSP126 low-emission scenario. For each model, we downloaded 3-hourly surface downwelling shortwave radiation (*rsds*), near-surface air temperature (*tas*), and zonal and meridional wind components (*uas*, *vas*). Most models provided data for only one realization, while only four models offered multiple realizations for all the four variables.

NO.	Model Name	Institute (Country)	Resolution	Realization
1	AWI-CM-1-1-MR	Alfred Wegener Institute (Germany)	0.9 × 0.9	r1i1p1f1
2	BCC-CSM2-MR	Beijing Climate Center (China)	1.1 × 1.1	r1i1p1f1
3	CanESM5	Canadian Centre for Climate Modelling and Analysis (Canada)	2.8 × 2.8	r1i1p2f1
4	CMCC-CM2-SR5	Euro-Mediterranean Centre on Climate Change (Italy)	0.9 × 1.3	r1i1p1f1
5	CMCC-ESM2	Euro-Mediterranean Centre on Climate Change (Italy)	0.9 × 1.3	r1i1p1f1
6	CNRM-CM6-1	Centre National de Recherches Météorologiques - Centre Européen de Recherche et Formation Avancée en Calcul Scientifique (France)	1.4 × 1.4	r1i1p1f2
7	CNRM-ESM2-1	Centre National de Recherches Météorologiques - Centre Européen de Recherche et Formation Avancée en Calcul Scientifique (France)	1.4 × 1.4	r1i1p1f2
8	EC-Earth3	Consortium of various institutions from Spain, Italy, Denmark, Finland, Germany, Ireland, Portugal, Netherlands, Norway, UK, Belgium, and Sweden (Europe)	0.7 × 0.7	r1i1p1f1
9	EC-Earth3-Veg	Consortium of various institutions from Spain, Italy, Denmark, Finland, Germany, Ireland, Portugal, Netherlands, Norway, UK, Belgium, and Sweden (Europe)	0.7 × 0.7	r1i1p1f1
10	GFDL-ESM4	National Oceanic and Atmospheric Administration - Geophysical Fluid Dynamics Laboratory (USA)	1.0 × 1.3	r1i1p1f1
11	GISS-E2-1-G	National Aeronautics and Space Administration - Goddard Institute for Space Studies (USA)	2.0 × 2.5	r1i1p1f2
12	IITM-ESM	Centre for Climate Change Research - Indian Institute of Tropical Meteorology (India)	1.9 × 1.9	r1i1p1f1
13	KIOST-ESM	Korea Institute of Ocean Science and Technology (Korea)	1.9 × 1.9	r1i1p1f1
14	MIROC6	Model for Interdisciplinary Research on Climate (Japan)	1.4 × 1.4	r1i1p1f1, r2i1p1f1, r3i1p1f1
15	MIROC-ES2L	Model for Interdisciplinary Research on Climate (Japan)	2.8 × 2.8	r1i1p1f2, r2i1p1f2, r3i1p1f2, r4i1p1f2, r5i1p1f2
16	MPI-ESM1-2-HR	Max Planck Institute for Meteorology (Germany)	0.9 × 0.9	r1i1p1f1
17	MPI-ESM1-2-LR	Max Planck Institute for Meteorology (Germany)	1.8 × 1.9	r1i1p1f1
18	MRI-ESM2-0	Meteorological Research Institute (Japan)	1.1 × 1.1	r1i1p1f1, r2i1p1f1, r3i1p1f1, r4i1p1f1, r5i1p1f1
19	NESM3	Nanjing University of Information Science and Technology (China)	1.8 × 1.9	r1i1p1f1, r2i1p1f1

Table S4. **Meteorology and emission datasets used in driving GEOS-Chem**. See Methods for details.

	Categories	Description	References
Meteorological fields	MERRA2	Spatial resolution: 0.5°×0.625° Temporal frame: 2014-2019	Ref [28]
	GISS ModelE2	Spatial resolution: 2°×2° Temporal frame: 2046-2049	Ref [29]
Anthropogenic emissions (power plants excluded)	Ambitious-pollution-1.5°C-goal	2050	Ref [1,15]
	Ambitious-pollution-2°C-goal	2050	
Power plant emissions	Strong and weak end-of-pipe emission control technologies	2050	See Table S2 for details

Table S5. Air quality thresholds and the change in frequency of extreme pollution hours due to fossil fuel plant emissions in northern and southern China.

Categories	Regions (domains in Fig. 2-4)	Thresholds †	Zero-fossil benchmark		With-fossil scenario (Changes compared to the zero-fossil benchmark)	
			Mean concentration	Number of extreme pollution hours or days	Mean concentration	Number of extreme pollution hours or days
Hourly $PM_{2.5}$	North	25 μg m^{-3}	13.8 μg m^{-3}	503 hours a^{-1}	+1.2 μg m^{-3}	+52%
	South	15 μg m^{-3}	8.7 μg m^{-3}	371 hours a^{-1}	+0.9 μg m^{-3}	+117%
Hourly O_3	North	50 ppb	31.4 ppb	427 hours a^{-1}	+0.1 ppb	+38%
	South	35 ppb	24.7 ppb	261 hours a^{-1}	+0.9 ppb	+100%
Daily mean $PM_{2.5}$	North	23 μg m^{-3}	13.8 μg m^{-3}	25.0 days a^{-1}	+1.2 μg m^{-3}	+47%
	South	14 μg m^{-3}	8.7 μg m^{-3}	15.0 days a^{-1}	+0.9 μg m^{-3}	+144%
Daily MDA8 O_3	North	53 ppb	36.7 ppb	22.2 days a^{-1}	+0.9 ppb	+65%
	South	36 ppb	27.5 ppb	16.8 days a^{-1}	+1.9 ppb	+118%

† This column defines the thresholds used to identify extreme pollution hours (for hourly data) or days (for daily data). These values correspond to approximately the 90th percentile of the time series under the with-fossil scenario.

Table S6. Different costs used in calculating the levelized cost of energy (LCOE). See Methods for more details about the calculation.

Categories	Description	References
Onshore wind installation cost in 2050	803 USD	Chen et al.[21]
Onshore wind operation cost	1.5%	
Offshore wind installation cost in 2050	1379 USD	
Offshore wind operation cost	1.5%	
Solar installation cost in 2050	475 USD	
Solar operation cost	2%	

Table S7. Inputs for calculating fuel, health, and GHG costs from fossil fuel power plants.

	Categories	Coal†	Gas	Biomass
Fossil fuel Cost	Fuel price ¶ ($ ton^{-1} for coal and biomass, $ m^{-3} for gas)	49 (ref [30])	0.169 (ref [30])	60 (ref [31])
	Fuel use rates (g kWh^{-1} for coal and biomass, m^3 kWh^{-1} for gas)	281 (ref [3])	0.213 (ref [3])	511 (ref [31])§
	Fuel cost ($ kWh^{-1})	0.0138	0.0361	0.0307
Health Cost	Health cost ($ kWh^{-1}) ‡ (calculated in this study)	0.0438±0.011	0.0176±0.004	0.0438±0.011
Greenhouse gas cost	CO_2 emission factors (g kWh^{-1})	773 (ref [3])	455 (ref [3])	0 (ref [32])
	Greenhouse gas cost (CO_2 price at $52 ton^{-1}) (ref [30])	0.0402	0.0237	0

¶ In this scenario, fuel prices for China in 2050 are based on the Net Zero Emissions (NZE) scenario from the International Energy Agency (Table 2.3 in ref [30]). For biomass, where NZE data are unavailable, we use China-specific projections from ref [31].

†For coal-fired power plants, fuel use rates and CO_2 emission factors correspond to large-sized thermal units (Table S17 in ref [3]).

‡Health costs are estimated using the emission factors listed in Table 1 (see details in Methods). Due to the lack of reported emission factors for biomass power plants, we assume biomass plants share the same emission factors as coal-fired plants. Sensitivity experiments are conducted to quantify air quality responses to emission changes from coal/biomass and gas plants, and the resulting health costs are derived using epidemiological concentration–response (C–R) functions (see Methods for details). Health costs for each energy scenario (Scenarios 1–24) are calculated as electricity-generation–weighted averages across fossil fuel types within each scenario.

§Values represent averages across solid fuels, including farmed trees, herbaceous biomass, corn stover, forest residues, sugarcane bagasse, and petroleum coke.

Table S8 Sensitivity experiments conducted for solving the optimal level of renewable scalability.

Experiments	Plant lifetime (years)	Investment discount rates	Fuel prices	Share of fossil fuel generation
The baseline	25	8%	Low	10.5
Varying wind+solar plant lifetimes	20	8%	Low	11.5%
	30	8%	Low	10.0%
	35	8%	Low	9.7%
Varying discount rates	25	5%	Low	8.5%
	25	6%	Low	9.0%
	25	7%	Low	9.7%
Higher fossil fuel prices¶	25	8%	High	8.8%

¶ Here, fuel prices are based on the Announced Pledges Scenario (APS) from the International Energy Agency (Table 2.3 in ref [30]), which higher that in the Net Zero Emissions (NZE) scenario. The fuel price is \$61 ton^{-1} for coal and \$0.219 m^{-3} for gas. For biomass, we adopt a higher estimate from ref [31] at \$100 ton^{-1}.

Table S9. Comparison of health costs from fossil fuel power plant emissions between this study and Chen et al. (2024). Part 1: Emission factors used in the two studies.

	Chen et al. [7]		This work (in the 2050, strong end-of-pipe emission control)	
Species	Coal (g/kWh)	Gas (g/kWh)	Coal (g/kWh)	Gas (g/kWh)
Description	These emission factors are for coal-plants in the year 2017 (Table S7 in Chen et al. [7])	These emissions factors are for gas plants planned future, which have very low values	From the DPEC inventory	From the DPEC inventory
SO_2	0.22-0.60 (based on regions)	0.0066	0.15	0
NO_x	0.8-1.2	0.107	0.27	0.23
$PM_{2.5}$	0.09-0.3	0.0048	0.02	0

Table S10. Comparison of health costs from fossil fuel power plant emissions between this study and Chen et al. (2024). Part 2: Stepwise decomposition illustrating how our health costs are compared with those in Chen et al. (2024). See Text S5 for more details. (unit: USD cents kWh^{-1}, health costs per kWh fossil fuel generation)

		Chen et al. [7]	This work (Experiment 0)	This work (Experiment 1)	This work (Experiment 2)	This work (Experiment 3)
	Population years	2020	2050	2020	2020	2020
	Emission factors	2017	2050	2050	Consistent with Chen et al.	Consistent with Chen et al.
	VSL values	Based a US study	Age-variant, China-specific VSL	Age-variant, China-specific VSL	Age-variant, China-specific VSL	Consistent with Chen et al.
Coal plants	Health Cost from $PM_{2.5}$	12.3	3.66	0.65	1.89	13.2
	Health Cost from O_3	Not calculated	0.72	0.09	0.34	2.44
Gas plants	Health Cost from $PM_{2.5}$	0.77	1.53	0.27	0.14	0.96
	Health Cost from O_3	Not calculated	0.23	0.03	0.015	0.11

Table S11. Suitability (%) of different land types for wind and solar installation (ref [3]).

%	PV	Onshore Wind
Forests	0	0
Closed Shrubland	15	100
Open Shrubland	15	100
Woody savanna	15	100
Savanna	15	100
Grassland	15	100
Wetland	0	0
Croplands	0	100
Urban	0	0
Vegetation mosaics	0	100
Snow, ice	10	0
Deserts	15	100
Water bodies	0	0

References

1. Cheng, J. *et al.* Pathways of China's PM2.5 air quality 2015–2060 in the context of carbon neutrality. *Natl. Sci. Rev.* **8**, nwab078 (2021).
2. Zhou, J. *et al.* Modeling and configuration optimization of the natural gas-wind-photovoltaic-hydrogen integrated energy system: A novel deviation satisfaction strategy. *Energy Convers. Manag.* **243**, 114340 (2021).
3. Chen, X. *et al.* Pathway toward carbon-neutral electrical systems in China by mid-century with negative CO2 abatement costs informed by high-resolution modeling. *Joule* **5**, 2715–2741 (2021).
4. Horton, D. E., Skinner, C. B., Singh, D. & Diffenbaugh, N. S. Occurrence and persistence of future atmospheric stagnation events. *Nat. Clim. Change* **4**, 698–703 (2014).
5. Wang, J. & Angell, J. Air stagnation climatology for the United States (1948–1998). NOAA/Air Resources Laboratory ATLAS 1, 76 pp. (1999).
6. Wang, X., Dickinson, R. E., Su, L., Zhou, C. & Wang, K. PM2.5 Pollution in China and How It Has Been Exacerbated by Terrain and Meteorological Conditions. *Bull. Am. Meteorol. Soc.* **99**, 105–119 (2018).
7. Chen, Y. *et al.* Maximizing the environmental benefits of gas power development in China: A multidisciplinary modeling approach. *iScience* **27**, 111041 (2024).
8. Tong, D. *et al.* Targeted emission reductions from global super-polluting power plant units. *Nat. Sustain.* **1**, 59–68 (2018).
9. Hammitt, J. K. & Robinson, L. A. The Income Elasticity of the Value per Statistical Life: Transferring Estimates between High and Low Income Populations. *J. Benefit-Cost Anal.* **2**, 1–29 (2011).
10. Yin, H. *et al.* Population ageing and deaths attributable to ambient PM2·5 pollution: a global analysis of economic cost. *Lancet Planet. Health* **5**, e356–e367 (2021).
11. Cao, C. *et al.* Estimating the value of a statistical life in China: A contingent valuation study in six representative cities. *Chin. J. Popul. Resour. Environ.* **21**, 269–278 (2023).
12. Lu, T. *et al.* India's potential for integrating solar and on- and offshore wind power into its energy system. *Nat. Commun.* **11**, 4750 (2020).
13. Liu, F. *et al.* High-resolution inventory of technologies, activities, and emissions of coal-fired power plants in China from 1990 to 2010. *Atmospheric Chem. Phys.* **15**, 13299–13317 (2015).
14. Peng, L. *et al.* Alternative-energy-vehicles deployment delivers climate, air quality, and health co-benefits when coupled with decarbonizing power generation in China. *One Earth* **4**, 1127–1140 (2021).
15. Tong, D. *et al.* Dynamic projection of anthropogenic emissions in China: methodology and 2015–2050 emission pathways under a range of socio-economic, climate policy, and pollution control scenarios. *Atmospheric Chem. Phys.* **20**, 5729–5757 (2020).
16. Cheng, J. *et al.* Comparison of Current and Future PM $_{2.5}$ Air Quality in China Under CMIP6 and DPEC Emission Scenarios. *Geophys. Res. Lett.* **48**, (2021).
17. Hudman, R. C. *et al.* Steps towards a mechanistic model of global soil nitric oxide emissions: implementation and space based-constraints. *Atmospheric Chem. Phys.* **12**, 7779–7795 (2012).
18. Guenther, A. B. *et al.* The Model of Emissions of Gases and Aerosols from Nature version 2.1 (MEGAN2.1): an extended and updated framework for modeling biogenic emissions. *Geosci. Model Dev.* **5**, 1471–1492 (2012).
19. Li, K. *et al.* A two-pollutant strategy for improving ozone and particulate air quality in China. *Nat. Geosci.* **12**, 906–910 (2019).
20. Sillman, S. The use of NO_y, H_2O_2, and HNO_3 as indicators for ozone-NO_x -hydrocarbon sensitivity in urban locations. *J. Geophys. Res. Atmospheres* **100**, 14175–14188 (1995).
21. Chen, S. *et al.* The Potential of Photovoltaics to Power the Belt and Road Initiative. *Joule* **3**, 1895–1912 (2019).
22. Wang, Y. *et al.* Accelerating the energy transition towards photovoltaic and wind in China. *Nature* **619**, 761–767 (2023).
23. Zhuo, Z. *et al.* Cost increase in the electricity supply to achieve carbon neutrality in China. *Nat. Commun.* **13**, 3172 (2022).
24. China Energy Foundation. China 2050 High Renewable Energy Penetration Scenario and Roadmap Study. (2015).
25. Zhang, S. & Chen, W. Assessing the energy transition in China towards carbon neutrality with a probabilistic framework. *Nat. Commun.* **13**, 87 (2022).
26. Fan, J.-L. *et al.* Co-firing plants with retrofitted carbon capture and storage for power-sector emissions mitigation. *Nat. Clim. Change* **13**, 807–815 (2023).
27. Ou, Y. *et al.* Deep mitigation of CO2 and non-CO2 greenhouse gases toward 1.5 °C and 2 °C futures. *Nat. Commun.* **12**, 6245 (2021).
28. Gelaro, R. *et al.* The Modern-Era Retrospective Analysis for Research and Applications, Version 2 (MERRA-2). *J. Clim.* **30**, 5419–5454 (2017).

29. Murray, L. T., Leibensperger, E. M., Orbe, C., Mickley, L. J. & Sulprizio, M. GCAP 2.0: a global 3-D chemical-transport model framework for past, present, and future climate scenarios. *Geosci. Model Dev.* **14**, 5789–5823 (2021).
30. International Energy Agency. World Energy Outlook 2024. https://www.iea.org/reports/world-energy-outlook-2024 (2024).
31. IRENA. Biomass for Heat and Power. https://www.irena.org/publications/2015/Jan/Biomass-for-Heat-and-Power (2015).
32. National Renewable Energy Laboratory. Life Cycle Greenhouse Gas Emissions from Electricity Generation: Update. https://www.nrel.gov/docs/fy21osti/80580.pdf (2021).